

Herwig++ 1.0: An Event Generator for e^+e^- Annihilation

**Stefan Gieseke[†], Alberto Ribon[‡], Michael H Seymour^{*}, Philip Stephens[†],
Bryan Webber^{†,§}**

[†]*Cavendish Laboratory, University of Cambridge, Madingley Road, Cambridge,
CB3 0HE, United Kingdom.*

[‡]*EP Division, CERN, 1211 Geneva 23, Switzerland.*

^{*}*Theory Group, Department of Physics and Astronomy, Schuster Laboratory,
University of Manchester, Manchester M13 9PL, UK.*

[§]*TH Division, CERN, 1211 Geneva 23, Switzerland.*

ABSTRACT: Results from the new Monte Carlo event generator **Herwig++** are presented. This first version simulates Hadron Emission Reactions With Interfering Gluons in electron–positron annihilation. The parton shower evolution is carried out using new evolution variables suited to describing radiation from heavy quarks as well as light partons. The partonic final state is fragmented into hadrons by means of an improved cluster hadronization model. The results are compared with a wide variety of data from LEP and SLC.

KEYWORDS: Quantum Chromodynamics, Monte Carlo Event Generator, Parton Shower, Hadronization, Heavy Quark Physics.

Contents

1. Introduction	2
2. Main features of the code	2
2.1 Parton shower	3
2.2 Hadronization and decay	4
3. The parton shower in detail	4
3.1 Hard matrix element correction	4
3.2 Initial conditions	4
3.3 Parton splittings and kinematics	5
3.4 Parametrization of Q_g	7
3.5 Single branching process	7
3.6 Angular ordering	9
3.7 Soft matrix element correction	9
3.8 Reconstruction of kinematics	10
4. The cluster hadronization in detail	10
4.1 Cluster formation	11
4.2 Cluster decays	12
4.3 Hadron decays	13
5. Observables	14
5.1 Observables considered	14
5.2 Analysis	15
5.3 Strategy	16
6. Results	16
6.1 Hadron multiplicities	16
6.2 Jet multiplicity	17
6.3 Jet rates and Y_n distributions	17
6.4 Event shapes	18
6.5 Four jet angles	18
6.6 Single particle distributions	19
6.7 Identified hadron spectra	19
6.8 B fragmentation function	19
6.9 Overall results	19

1. Introduction

The new generation of high energy colliders such as the Large Hadron Collider (LHC) or a future linear collider (NLC) require new tools for the simulation of signals and backgrounds. The widely used event generators HERWIG [1] and PYTHIA [2] underwent tremendous development during the LEP era and have reached the limit of reasonable maintenance in the future. Therefore these programs (Pythia7) [3] as well as new projects, like SHERPA [4], are being completely (re-)developed in the object-oriented programming language C++.

In this paper we present results from the new Monte Carlo event generator **Herwig++** as the first step in the redevelopment of HERWIG. The generator will be used here to simulate e^+e^- annihilation events. In order to have full control of the basic physics steps that are simulated, we need to put the new generator on a firm basis with respect to LEP and SLC results before we go on to upgrade it to initial-state showers and the other requirements for the simulation of lepton-hadron and hadron-hadron collisions. Therefore we have tested the predictions of the generator against a wide range of observables that have been measured at LEP and SLC, and have explored the sensitivity to the most important parameters and cutoffs. We did not perform a high-precision tuning: our aim here is rather to describe the program and to show that it is able to give results as acceptable as those generated by its predecessor HERWIG for a reasonable choice of parameters.

2. Main features of the code

The details of **Herwig++** will be described in conjunction with the release of the code [5]. The main stages of the simulation of e^+e^- annihilation are the same as in HERWIG [1]. However, in comparison to its predecessor, **Herwig++** features a new parton shower and an improved cluster hadronization model. At present, hadronic decays are implemented in the same fashion as they were in HERWIG.

The program is based on the Toolkit for High Energy Physics Event Generation (**ThePEG**) [7] and the Class Library for High Energy Physics (**CLHEP**) [8]. They are utilized in order to take advantage of the extended general functionality they can provide. The usage of **ThePEG** unifies the event generation framework with that of **Pythia7**. This will provide benefits for the user, as the user interface, event storage etc. will appear to be the same. The implementations of the physics models, however, are completely different and independent from each other.

Our simulation starts with an initial hard process $e^+e^- \rightarrow (\gamma^*, Z^0) \rightarrow q\bar{q} + \gamma\gamma$. The final state photons simulate QED radiation from the initial state, so that a radiative return can be properly simulated. For the present paper we shall only be interested in the details of the QCD parton shower in the final state. The final-state parton shower starts with a quark and antiquark that carry momenta p_q and $p_{\bar{q}}$, respectively, and have an invariant mass squared of $Q^2 = (p_q + p_{\bar{q}})^2$. The only detail we are concerned with in relation to initial-state radiation is that the centre-of-mass frame of the $q\bar{q}$ -pair is slightly boosted with respect to the collider laboratory frame and that Q may be different from the e^+e^- centre-of-mass energy. We have made sure that the applied cuts on the energy of the annihilating e^+e^- subsystem are the same as those used in the experimental analyses.

2.1 Parton shower

The partonic evolution from the large scale of the hard collision process down to hadronic scales via the coherent emission of partons, mainly gluons, is simulated on the basis of the Sudakov form factor. Starting from the hard process scale Q_0 , subsequent emissions at scales Q_i and momentum fractions z_i are randomly generated as a Markov chain on the basis of the soft and collinear approximation to partonic matrix elements. Details are described in chapter 5 of [9]. In **Herwig++** we have chosen a new framework of variables, generically called (\tilde{q}, z) . Here, \tilde{q} is a scale that appears naturally in the collinear approximation of massive partonic matrix elements and generalizes the evolution variable of HERWIG to the evolution of massive quarks. z is a relative momentum fraction; the evolution is carried out in terms of the Sudakov decomposition of momenta in the frame where the respective colour partners are back-to-back. As in HERWIG, the use of the new variables allows for an inherent angular ordering of the parton cascade, which simulates coherence effects in soft gluon emission. The details of the underlying formalism are described elsewhere [10].

The most important parameter of the parton shower that we will be concerned with in this paper is the cutoff parameter Q_g , which regularizes the soft gluon singularity in the splitting functions and determines the termination of the parton shower. Less important but relevant in extreme cases is the treatment of the strong coupling constant at low scales. We have parametrized $\alpha_S(Q)$ below a small scale $Q_{\min} > \Lambda_{QCD}$ in different ways. We keep Q_{\min} generally to be of the order of 1 GeV, where we expect non-perturbative effects to become relevant. Below that scale $\alpha_S(Q)$ can optionally be

- set to zero, $\alpha_S(Q < Q_{\min}) = 0$,
- frozen, $\alpha_S(Q < Q_{\min}) = \alpha_S(Q_{\min})$,
- linearly interpolated in Q , between 0 and $\alpha_S(Q_{\min})$,
- quadratically interpolated in Q , between 0 and $\alpha_S(Q_{\min})$.

We put the final partons of the shower evolution on their constituent mass shells, since the non-perturbative cluster hadronization will take over at this scale, so we usually have kinematical constraints that keep Q above Q_{\min} , in which case the treatment below Q_{\min} is irrelevant. Typically, $\alpha_S(Q_{\min}) \sim 1$ here.

2.2 Hadronization and decay

The partonic final state is turned into a hadronic final state within the framework of the cluster hadronization model of HERWIG [11]. In order to address some shortcomings [12] a new cluster hadronization model ¹ has been created for **Herwig++**, which is discussed in sec. 4. The emerging hadrons are possibly unstable and eventually decay. The decay matrix elements and modes correspond to those in HERWIG.

3. The parton shower in detail

3.1 Hard matrix element correction

Before we begin the parton shower evolution, but after obtaining the final state $q\bar{q}$ -pair from the hard process, we decide whether or not a so-called hard matrix element correction will be applied. In order to do so, we decompose the $q\bar{q}g$ -phase space into regions that will be covered by the parton shower emissions and a ‘dead’ region that, based on our choice of evolution variables and initial conditions, is never populated by first parton shower emissions (see [10]). To take into account gluon emissions into the dead region we generate a pair of three-body phase-space variables x, \bar{x} according to the first order QCD matrix element. However, we only accept emissions into the dead region of phase space at a rate that is given by the QCD matrix element, that is, only 3 % of all emissions are corrected by the hard matrix element at all. Once we accept an additional hard gluon emission, we replace the $q\bar{q}$ -final state with the $q\bar{q}g$ final state. We keep the orientation of either the quark or antiquark with weights x^2 and \bar{x}^2 respectively, resulting in properly oriented three-jet events apart from finite mass effects [14]. In this way, we take into account the most important subleading higher-order corrections that are not enhanced by additional soft or collinear logarithms.

3.2 Initial conditions

Having completed the hard matrix element correction, the next task is to determine the initial conditions for the parton shower evolution. For every particle a we determine the colour partner or, more generally, the gauge ‘charge’ partner \bar{a} . In the case of a $q\bar{q}$ final state there is no ambiguity, whereas the gluon in $q\bar{q}g$ is assigned the quark or the antiquark with equal probability.

¹A new cluster hadronization model that addresses some of these shortcomings is also a feature of SHERPA [13].

For different interactions there can be different ‘charge’ partners. In our case we have also implemented collinearly enhanced photon emission from charged particles. In the case of the $q\bar{q}g$ final state the gluon doesn’t radiate photons and the only two charge partners are the quark and the antiquark. The remaining parts of the shower evolution are carried out in exactly the same way. Different sorts of interaction just add another splitting possibility for a given particle, which will compete with the others for the next possible splitting that occurs.

Once the colour partners are determined, we fix the shower kinematics and the initial evolution scale. As explained in detail in [10], the shower evolution of a particle a is carried out in a Sudakov basis,

$$q = \alpha p_a + \beta n_{\bar{a}} + q_{\perp}, \quad (3.1)$$

where p_a is the momentum of particle a with (current) mass-squared $p_a^2 = m_a^2$, $n_{\bar{a}}$ is a lightlike vector in the ‘backwards’ direction, along the momentum $p_{\bar{a}}$ of the partner \bar{a} , and q_{\perp} is the transverse momentum, $q_{\perp} \cdot p_a = q_{\perp} \cdot n_{\bar{a}} = 0$. In the centre-of-mass frame of a and \bar{a} we have $p_a = \frac{1}{2}Q(1, \mathbf{v})$ and we set $n_{\bar{a}} = \frac{1}{2}Q(v, -\mathbf{v})$, $q_{\perp} = (0, \mathbf{q}_{\perp})$ with $\mathbf{q}_{\perp} \cdot \mathbf{v} = 0$. Given this basis, we calculate the initial evolution scale for each particle as

$$\tilde{q}_{\text{ini}}^2 = (p_a + p_{\bar{a}}) \cdot (p_a + n_{\bar{a}}) = \frac{1}{2}Q^2(1 + v). \quad (3.2)$$

We note that this is the most symmetric choice of initial conditions (see [10]). In the $q\bar{q}$ -case, this choice starts the evolution of quark and antiquark at the same scale. We could as well choose another pair of evolution scales. If we do so, however, we make sure that the phase space region of soft gluon emission is covered uniquely and smoothly with the radiation from the two partners [10]. For later kinematic reconstruction we have to store the momenta p_i of the outgoing partons at this stage.

3.3 Parton splittings and kinematics

Starting from the evolution scale $\tilde{q}_i = \tilde{q}_{\text{ini}}$ we now carry out the parton shower evolution for each final state particle separately. For every possible splitting $a \rightarrow bc$ of particle a we determine the scale of the next branching \tilde{q}_{i+1} based on the Sudakov form factor

$$S_{ba}(\tilde{q}_i, \tilde{q}_{i+1}) = \frac{\Delta_{ba}(\tilde{q}_c, \tilde{q}_i)}{\Delta_{ba}(\tilde{q}_c, \tilde{q}_{i+1})}, \quad (3.3)$$

where

$$\Delta_{ba}(\tilde{q}_c, \tilde{q}) = \exp \left\{ - \int_{\tilde{q}_c}^{\tilde{q}} \frac{d\tilde{q}^2}{\tilde{q}^2} \int dz \frac{\alpha_S(z, \tilde{q})}{2\pi} P_{ba}(z, \tilde{q}) \Theta(\mathbf{p}_{\perp} > 0) \right\}. \quad (3.4)$$

\tilde{q}_c is the lower cutoff of the parton shower which, by default, is taken to be the nonperturbative gluon mass $m_g = 750 \text{ MeV}$. $\alpha_S(z, \tilde{q})$ is the running coupling in the

case of QCD evolution and generally depends on the evolution scale and momentum fraction. We choose $z(1-z)\tilde{q}$ as the argument of the running coupling which reduces to the transverse momentum \mathbf{q}_\perp in the massless case. $P_{ba}(z, \tilde{q})$ are the quasi collinear splitting functions that depend on the evolution scale in the case of massive partons [15]. For QCD branchings they are

$$P_{qq}(z, \tilde{q}) = C_F \left[\frac{1+z^2}{1-z} - \frac{2m_a^2}{z(1-z)\tilde{q}^2} \right], \quad (3.5)$$

$$P_{qg}(z, \tilde{q}) = T_R \left[1 - 2z(1-z) + \frac{2m_a^2}{z(1-z)\tilde{q}^2} \right], \quad (3.6)$$

$$P_{gg}(z, \tilde{q}) = C_A \left[\frac{z}{1-z} + \frac{1-z}{z} + z(1-z) \right]. \quad (3.7)$$

Similarly, for the branching $q \rightarrow q\gamma$, ignoring the parton mass, we have,

$$P_{q\gamma}^\gamma(z, \tilde{q}) = e_a^2 \frac{1+z^2}{1-z}, \quad (3.8)$$

with e_a being the electric charge of the parton in units of the elementary charge. Of course we have to take the fine structure constant α_{em} in eq. (3.4) in this case. $\Theta(\mathbf{q}_\perp > 0)$ limits the phase space to the region where it is possible to reconstruct the transverse momentum \mathbf{p}_\perp from the evolution variables (\tilde{q}, z) , which is a complicated and implicit function in our case. However, using the veto algorithm described below we do not need to know the phase space boundary explicitly.

The evolution variables \tilde{q} and z determine the kinematics of the parton shower. The momentum fraction z is simply the ratio of the Sudakov variables α in eq. (3.1) for the parent and daughter parton,

$$\alpha_{i+1} = z\alpha_i. \quad (3.9)$$

Based on its meaning in the quasi-collinear limit, \tilde{q} determines the relative transverse momentum as

$$|\mathbf{p}_\perp| = \sqrt{(1-z)^2(\tilde{q}^2 - \mu^2) - zQ_g^2} \quad (\text{quark branching}), \quad (3.10)$$

$$|\mathbf{p}_\perp| = \sqrt{z^2(1-z)^2\tilde{q}^2 - \mu^2} \quad (\text{gluon branching}), \quad (3.11)$$

where

$$\mu = \max(m_a, Q_g), \quad (3.12)$$

when a quark of mass a is involved in the branching and simply $\mu = Q_g$ for the splitting $g \rightarrow gg$. Here we have introduced the cutoff Q_g in order to regularize the soft gluon singularities in the splitting function. The relative transverse momentum \mathbf{p}_\perp is related to the Sudakov variables (3.1) of the parton branching as

$$\mathbf{p}_\perp = \mathbf{q}_{\perp i+1} - z\mathbf{q}_{\perp i}. \quad (3.13)$$

From eqs. (3.10) and (3.11) we immediately get the phase space constraint for \mathbf{p}_\perp in eq. (3.4). We require z to correspond to a real value of \mathbf{p}_\perp . For gluon splittings we explicitly obtain

$$z_- < z < z_+, \quad z_\pm = \frac{1}{2} \left(1 \pm \sqrt{1 - \frac{4\mu}{\tilde{q}}} \right) \quad \text{and} \quad \tilde{q} > 4\mu. \quad (3.14)$$

For quark splittings the phase space boundary is the solution of a cubic equation but the allowed z range always lies within

$$\frac{\mu}{\tilde{q}} < z < 1 - \frac{Q_g}{\tilde{q}}. \quad (3.15)$$

Therefore it is simplest to generate z within this range and reject those values that lie outside phase space. Finally, it takes an azimuthal angle ϕ , which is currently chosen randomly and may later be related to spin correlations [16], to complete the four-momenta of the parton shower in a final kinematic reconstruction.

3.4 Parametrization of Q_g

We introduced the cutoff parameter Q_g quite naturally as a gluon virtuality into the shower kinematics. Considering the phase space that is available to the parton shower, we would expect a natural threshold in \tilde{q} of the order of $m_q + Q_g$. In contrast, we find from eq. (3.10) that the actual threshold behaves approximately as $Q_{\text{thr}} = 1.15(m_q + 2Q_g)$. Hence, we find that, particularly for heavy quarks the phase space limit is well above our expectation.

There is no reason why Q_g should be kept as the same parameter for all quark flavours. Therefore, we have chosen to parametrize the threshold for different flavours in terms of a unique parameter δ as

$$Q_g = \frac{\delta - 0.3 m_q}{2.3}, \quad (3.16)$$

which leaves us with a threshold $Q_{\text{thr}} = 0.85 m_q + \delta$ for all flavours². The resulting phase space in \tilde{q} and z is then as shown in fig. 1. We show the dependence of our results on the parameter δ in most of the plots of sec. 6. In the case of gluon splitting m_q is the mass of the splitting products, i.e. the quark mass in case of a $g \rightarrow q\bar{q}$ splitting or $m_q = 0$ in $g \rightarrow gg$ splitting.

3.5 Single branching process

For timelike (i.e. final state) branchings, given an initial scale \tilde{q}_i , the Sudakov form factor eq. (3.3) gives the probability for no branching above the scale \tilde{q}_{i+1} . Hence, $1 - S_{ab}(\tilde{q}_i, \tilde{q}_{i+1})$ is the probability for the next branching to happen above \tilde{q}_{i+1} and

²In principle, the coefficient of m_q could be a model parameter.

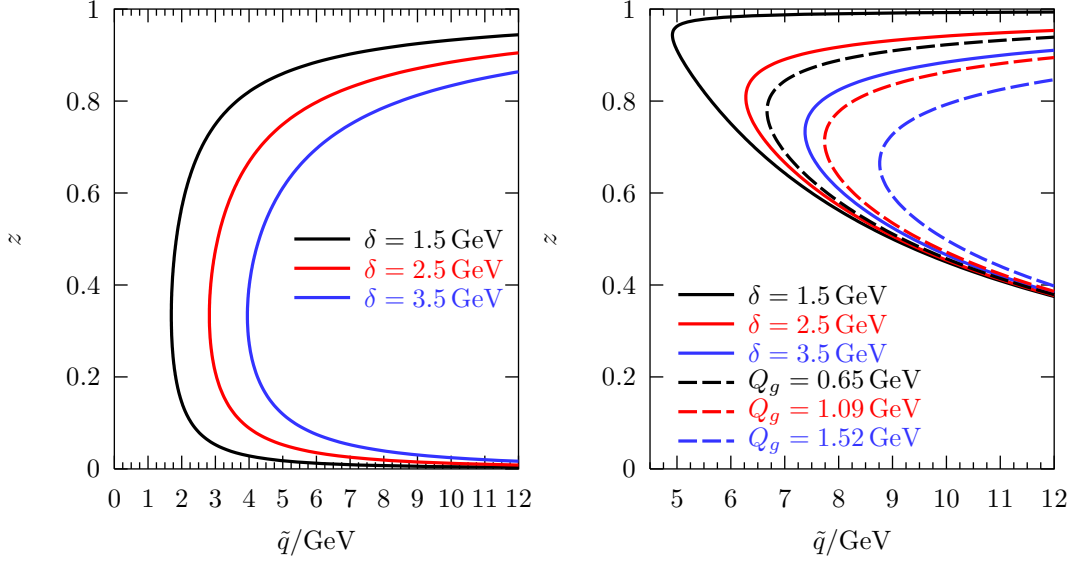


Figure 1: Available phase space of light (left) and b -quarks (right) for $q \rightarrow qg$ splitting for various values of Q_g and depending on the parametrization in terms of δ , eq. (3.16). The dashed lines on the right correspond to the same Q_g values as for the light quarks.

its derivative with respect to \tilde{q}_{i+1} is the probability density for the next branching to happen at the scale \tilde{q}_{i+1} .

We sample the next branching scale with the veto algorithm. We overestimate the integrands as follows. We take the absolute maximum of the relevant coupling α_{\max} as this is generally a very slowly varying function. The splitting functions are overestimated by

$$g_{qq}(z) = \frac{2C_F}{1-z}, \quad (3.17)$$

$$g_{qg}(z) = T_R, \quad (3.18)$$

$$g_{gg}(z) = C_A \left[\frac{1}{1-z} + \frac{1}{z} \right], \quad (3.19)$$

$$g_{qq}^\gamma(z) = \frac{2e_a^2}{1-z}, \quad (3.20)$$

in such a way that their integrals $G_{ba}(z)$ are invertible functions. Furthermore, they do not depend on \tilde{q} anymore. The phase space in z is overestimated by taking the maximum value of the evolution scale, \tilde{q}_i . From this, we calculate the limits in z from eq. (3.14) or (3.15), respectively. As we can now easily integrate and invert the exponent in eq. (3.4), we can sample values \tilde{q}_s and z_s . Then we subsequently apply vetoes with weights

$$w_1 = \Theta(\mathbf{p}_\perp > 0), \quad w_2 = \frac{P_{ba}(z, \tilde{q})}{g_{ba}(z)}, \quad w_3 = \frac{\alpha(z, \tilde{q})}{\alpha_{\max}}. \quad (3.21)$$

When all vetoes are passed, we have a scale $\tilde{q}_{i+1} = \tilde{q}_s$ and a momentum fraction z_s value. If not, we try to obtain a new branching, now starting at scale \tilde{q}_s , repeating until we either accepted a scale as the next branching scale or we obtain a scale $\tilde{q}_s < \tilde{q}_c$ at which we cannot resolve a parton any further.

In this way we calculate branching scales \tilde{q}_{i+1} for every possible splitting process for a given particle. The splitting with the largest scale of those above \tilde{q}_c is then taken to be the next branching. In this way we can easily include any type of branching.

3.6 Angular ordering

Once a parton is split its resolution scale \tilde{q}_i is still above the smallest resolution scale \tilde{q}_c . In order to have angular ordering we now calculate the subsequent branchings of its daughters as \tilde{q}_{i+1} and \tilde{k}_{i+1} with the conditions

$$\tilde{q}_{i+1} < z\tilde{q}_i \quad \tilde{k}_{i+1} < (1 - z)\tilde{q}_i. \quad (3.22)$$

This branching process is repeated until no more daughter particles are resolved at scales above the resolution scale \tilde{q}_c . Note that, for our choice of evolution variables, the parton shower is terminated because there is no more phase space available at low scales. The lower limit of evolution is normally given by the soft gluon cutoff Q_g (or δ) or the masses m of the branching particles (cf. fig. 1). However, when we choose very small cutoffs Q_g , which are in principle allowed, we apply the additional constraint $\tilde{q} > \tilde{q}_c$ on the shower termination.

3.7 Soft matrix element correction

As explained in sec. 3.1 we explicitly populate the ‘dead region’ of the $q\bar{q}g$ phase space according to the correct QCD matrix element. We also improve parton shower emissions within the shower regions of the phase space, as the parton shower might generate relatively hard gluon emissions which are not within the domain of validity of the quasi-collinear approximation anymore.

In order to do so, we keep track of the relative transverse momentum \mathbf{p}_\perp (cf. eqs. (3.10), (3.11)) that was generated during the parton shower evolution of one jet. Whenever we find that this transverse momentum is the largest that was generated during the evolution so far we apply a so-called soft matrix element correction [17].

We consider all previous gluon emissions as being infinitely soft in comparison to the one we are testing. This allows us to compute the three-body (i.e. $q\bar{q}g$) variables (x, \bar{x}) from the parton shower variables (\tilde{q}, z) and the respective Jacobian. Then we compare a random number with the ratio of the true matrix element to the parton shower approximation and reject the branching if the ratio is smaller. Clearly this requires the parton shower emission probability to be larger than the matrix element everywhere in phase space, which is true for this process and our choice of evolution variables.

3.8 Reconstruction of kinematics

As we generate the parton splittings $i \rightarrow (i+1)k$ we can calculate the α_{i+1} -component and the transverse momentum of the daughter parton $(i+1)$ using eqs. (3.9) and (3.13). The respective variables of the second particle k are simply obtained using $1-z$ and the difference of the transverse momenta of i and $(i+1)$. However, we can only reconstruct the β variables when we know the virtuality of each particle. This is done recursively once the parton shower evolution has terminated. The final-state particles are put on their constituent mass shells and then we obtain the beta components from

$$\beta = \frac{q^2 + \mathbf{q}_\perp^2 - \alpha^2 p^2}{2\alpha p \cdot n}, \quad (3.23)$$

where p and n are the Sudakov basis vectors of the shower. These were determined in the initial phase and remain fixed for each jet.

After the completion of the shower evolution of every parton j involved in the hard process, the jet parent partons are not on their mass shells $p_j^2 = m_j^2$ anymore. Instead, they have acquired virtualities q_j^2 . If the original momenta were given as $p_j = (\sqrt{\mathbf{p}_j^2 + m_j^2}, \mathbf{p}_j)$ in the centre-of-mass frame of the hard process, we want to preserve the total energy in this frame,

$$\sqrt{s} = \sum_{j=1}^n \sqrt{m_j^2 + \mathbf{p}_j^2}, \quad (3.24)$$

while we want to keep the sum of spatial momenta vanishing. As the jet parents have momenta $q_j = (E_j, \mathbf{q}_j)$ after the showering, we need some way to restore momentum conservation in a way that most smoothly preserves the internal properties of each jet.

The simplest way to do this so-called “momentum reshuffling” is to rescale the momentum of each jet with a common factor k that is determined implicitly from

$$\sqrt{s} = \sum_{j=1}^n \sqrt{q_j^2 + k\mathbf{p}_j^2}. \quad (3.25)$$

Then, for every jet we determine a Lorentz transformation such that

$$q_j = (E_j, \mathbf{q}_j) \xrightarrow{\text{boost}} q'_j = (E'_j, k\mathbf{p}_j). \quad (3.26)$$

Typically the rescaling parameters k are very close to unity and hence the resulting angles and boost parameters in eq. (3.26) are small.

4. The cluster hadronization in detail

The cluster hadronization has two main steps. The first is the cluster formation, in which all of the colour connected partons created in the shower are combined to

form clusters which are colour singlets. The other step is the decay of these colour singlet clusters into hadrons. The new model presented here only changes the second stage, how the cluster decays. The process of cluster formation remains identical to HERWIG, with the same set of parameters.

4.1 Cluster formation

The gluons in the partonic final state are split non-perturbatively into $q\bar{q}$ pairs. The choice of flavour is between the u, d and s flavours. The splitting is done with a simple isotropic decay where the gluon is given an effective gluon mass, $m_g > 2m_q$. The default value for m_g is 0.75 GeV.

Once we have a state of all on-shell quarks, the colour partners are combined into clusters. Owing to the colour-preconfinement property of the parton shower [18], the cluster mass distribution is independent of the nature and energy of the hard process to a good approximation. This can be seen in Figure 2 for light (uds) quark clusters and clusters containing a b quark separately.

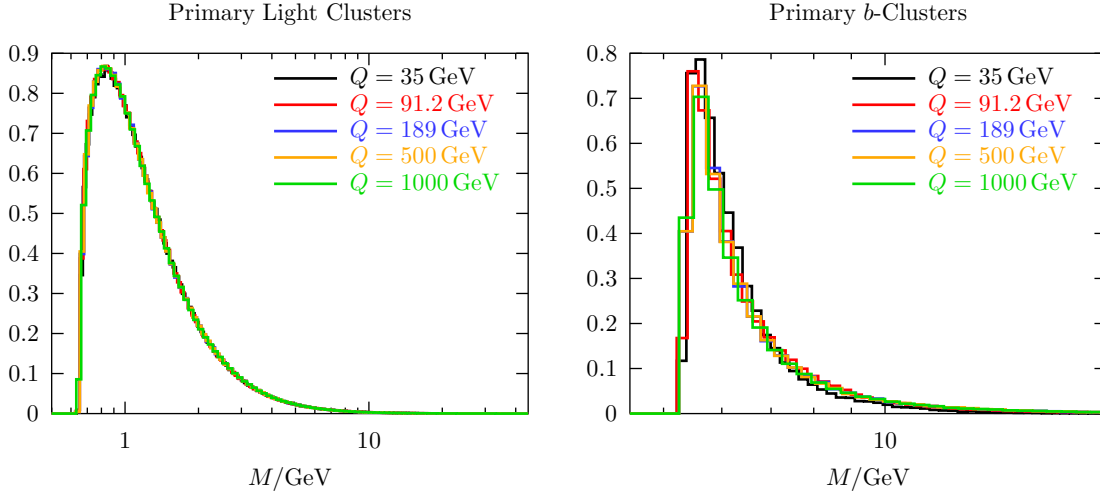


Figure 2: Primary cluster mass distribution in e^+e^- annihilation at various centre-of-mass energies Q for clusters containing only light quarks (left) and a b quark (right).

The hadronization model in HERWIG and Herwig++ also has a stage where some of these clusters are decayed into two new clusters, rather than directly to hadrons. This step is called cluster fission. The mass of a cluster is given by $M^2 = p^2$, where p is the momentum of the cluster. The cluster C is decayed into two new clusters C_1, C_2 if this mass does not satisfy the condition

$$M^{\text{Cl}_{\text{pow}}} < \text{Cl}_{\text{max}}^{\text{Cl}_{\text{pow}}} + \Sigma_c^{\text{Cl}_{\text{pow}}}, \quad (4.1)$$

where Cl_{pow} and Cl_{max} are parameters of the model and Σ_c is the sum of the masses of the constituent partons which form the cluster. If a cluster does decay into two

new clusters, a flavour is drawn from the vacuum. Again this is drawn from the u, d and s flavours. The mass of cluster i is drawn from the following distribution

$$M_i = \left[(M^P - (m_i + m_3)^P) r_i + (m_i + m_3)^P \right]^{1/P}, \quad (4.2)$$

where m_i is the mass of the constituent quark from the original cluster that is going into the new cluster and m_3 is the constituent mass of the flavour that was drawn from the vacuum. Here P is a parameter of the model and r_i is a random number. The value of P is given by PSPLT(1) if parton i is of u, d, s or c flavour and by PSPLT(2) for a cluster where parton i is of b flavour. The two masses are also correlated by the constraint that $M_1 + M_2 \leq M$. If this constraint is violated, a new flavour is drawn from the vacuum and two new cluster masses are drawn from the distribution (4.2). The decay kinematics is determined in the rest frame of C , as the original constituent quarks continue their movement in the same direction also when they are boosted into the rest frame of the new clusters C_1, C_2 . As all masses are given, the momenta of clusters and constituents are determined.

4.2 Cluster decays

The last stage of the hadronization is the cluster decays. The problem with the original HERWIG cluster decay model [11] can be shown as follows. The probability of accepting a decay of a cluster with flavours i, j into hadrons of type a, b is

$$P(a_{i,q}, b_{q,j} | i, j) = P_q P(a | i, q) P(b | q, j) P_{\text{PS}}(a, b). \quad (4.3)$$

Here P_q is the probability of drawing flavour q from the vacuum and P_{PS} is the probability due to phase space. The probabilities of interest are the other two. These have the form

$$P(a | i, j) = \frac{w_a}{N_{ij} M_{ij}}, \quad (4.4)$$

where w_a is a hadron specific weight, M_{ij} is the maximum weight of all the hadrons of flavour i, j and N_{ij} is the number of hadrons of flavour i, j in the model. We can see that the probabilities have a dependence on N_{ij} . As described in [12] this causes adverse side effects when new hadrons are added to the model. If we consider adding a new hadron of flavour $u\bar{d}$, for example, it will generally be heavier than those already present. This will suppress the probability of choosing a lighter $u\bar{d}$ meson as $N_{u\bar{d}}$ is increased. Therefore properties such as the charged to neutral pion ratio are controlled heavily by how many hadrons of a particular flavour are in the model.

To solve this problem a new construction of the probability was created in [12]. Instead of independently choosing the flavour from the vacuum and then choosing the hadrons, this is all combined into one distribution. The weight of one choice is

$$W(a_{i,q}, b_{q,j} | i, j) = P_q w_a w_b P_{\text{PS}}(a, b). \quad (4.5)$$

This gives the probability

$$P(a_{i,q}, b_{q,j}|i, j) = \frac{W(a_{i,q}, b_{q,j}|i, j)}{\sum_{q',c,d} W(c_{i,q'}, d_{q',j}|i, j)}. \quad (4.6)$$

Because P_{PS} is zero for heavy decay modes only accessible modes influence the probabilities. Unfortunately, this solution has a new problem in that the ratio of mesons to baryons is dictated by the number of available particles. Since there are many more mesons than baryons the denominator in eq. (4.6) is quite large and the total probability of choosing a baryonic decay mode is very small. So though this new approach is able to make quantities such as pion ratios independent of the number of hadrons in the model it fails to produce the correct amount of baryons.

The solution implemented in **Herwig++** is to treat the baryon sector independently from the meson sector. This is done by re-interpreting the parameter for the diquark weight, Pwt_{di} , to be the parameter that controls the frequency of drawing independently from the baryon sector. This is expressed as

$$P_B = \frac{\text{Pwt}_{\text{di}}}{\text{Pwt}_{\text{di}} + 1}. \quad (4.7)$$

So there is a probability P_B of choosing only from the baryon sector and a probability $P_M = 1 - P_B$ of choosing from the meson sector. The actual choice of hadrons is then made according to the probability

$$P(a_{i,q}, b_{q,j}|i, j) = \frac{W(a_{i,q}, b_{q,j}|i, j)}{\sum_{M/B} W(c_{i,q'}, d_{q',j}|i, j)}. \quad (4.8)$$

where the sum over M/B indicates only summing over the flavours that produce either mesons or baryons.

4.3 Hadron decays

Most of the hadrons created in the cluster hadronization are not stable and need to be decayed. At present, the decays in **Herwig++** are done in the same way as in **HERWIG**. Most decays are treated as simple n -body isotropic decays. Weak decays are done by either free particle $V - A$ matrix elements or bound quark $V - A$ matrix elements. Examples of these are $\tau^- \rightarrow e^- \bar{\nu}_e \nu_\tau$ and $K^- \rightarrow e^- \bar{\nu}_e \pi^0$, respectively.

Heavy hadrons, such as B mesons, are sometime decayed into partonic states. These states are then fed back into the shower and are re-showered and re-hadronized. There are two different types of heavy partonic decays. One is a weak decay, for which we use the same free or bound $V - A$ matrix elements as for the light mesons. This would occur, for example, in the decay $B^0 \rightarrow \bar{s} c \bar{c} d$. There are also quarkonium decays that have gluons as decay products, for example the decay $\eta_c \rightarrow gg$. These decays are done using the appropriate positronium matrix elements.

5. Observables

5.1 Observables considered

We considered the following observables in our study.

Event shape variables: Event shape distributions have been measured to very high accuracy at LEP and aim at resolving the properties of the parton shower quite deeply. In particular we have chosen the thrust (T), thrust major (M), thrust minor (m) and oblateness (O) as they are the most commonly used. In addition we look at the C -parameter and D -parameter as they are more sensitive to multijet events. We also look at the sphericity and planarity (S, P), which are calculated from the quadratic momentum tensor and therefore put more emphasis on 2-jet like events. Furthermore we look at the wide and narrow jet broadening measures (B_{\max}, B_{\min}), which are more sensitive to the transverse jet structure.

Jet multiplicity: The multiplicity of (mini-)jets in e^+e^- -collisions for different values of the jet resolution y_{cut} . We use the Durham- or k_{\perp} -clustering scheme [19] throughout the paper for jet observables. To be specific, for a given final state the jet measure

$$y_{ij} = \frac{2 \min(E_i^2, E_j^2)}{Q^2} (1 - \cos \theta_{ij}) \quad (5.1)$$

is calculated for every particle pair (i, j) . The particles with minimal jet measure are clustered such that the momentum of the clustered pseudo-particle is the sum of the four-momenta of the constituents. The jet multiplicity is then the number of pseudo-particles remaining when all $y_{ij} > y_{\text{cut}}$. This inclusive observable has been predicted and measured at LEP energies and will test the dynamics of the parton shower as well as the interface between parton shower and hadronization. We use the **KtJet**-package [20] that implements the above jet-finding algorithm in C++ and have written a simple wrapper around it in order to use it with our own particle record.

Jet fractions and Y_n : A closer look ‘into’ the jets is provided by considering the rates of jets at a given value of y_{cut} in the Durham scheme, $R_n = N_{n\text{-jet}}/N_{\text{evts}}$ for $n = 2$ up to $n = 6$ jets. We also look at the distributions of Y_n , the y_{cut} -values at which an $n + 1$ jet event is merged into an n -jet event in the Durham clustering scheme. Here we look at $n = 2$ up to $n = 5$. These distributions will not only probe the dynamics of the parton shower but also the hadronization model: at the lowest values of $y_{\text{cut}} \sim (\tilde{q}_c/Q)^2$ the dynamics is dominated by the latter.

Four-jet angles: A very interesting set of observables are the distributions of the angles between jets in four-jet events, χ_{BZ} , Φ_{KSW} , θ_{NR}^* and α_{34} , defined for example in ref. [21]. These angles are expected to be sensitive to the accuracy of the simulation of higher-order matrix elements.

Single particle distributions: Another interesting set of observables are the momentum distributions of final-state particles with respect to the event orientation. y^T is the rapidity distribution with respect to the thrust axis, $p_{\perp,\text{in}}^T$ and $p_{\perp,\text{out}}^T$ are the respective transverse momenta within and out of the event plane, defined by the thrust and thrust major axes. Without any reference to the event orientation, we look at the distribution of the momentum fraction $x_p = 2|\mathbf{p}|/Q$ and at $\xi_p = -\log x_p$ which displays better the effects of soft gluon coherence at small x_p .

Identified particle spectra: We consider the exclusive momentum distributions of π^\pm , K^\pm , p, \bar{p} and $\Lambda, \bar{\Lambda}$. These are generally expected to be sensitive to the hadronization model. In all cases except $\Lambda, \bar{\Lambda}$ we can compare with data on the momentum distributions from uds , c and b events separately.

Hadron multiplicities: The charged particle multiplicity distribution and the average multiplicities of a wide range of hadron species were taken to test the overall flow of quantum numbers through the different stages of simulation. The improved cluster hadronization model can be tested thoroughly against these observables.

B fragmentation function: The energy fraction of B -hadrons is taken as a test for the new parton shower which is specifically designed to improve the description of heavy quark observables with respect to the description in HERWIG.

The above list of observables has proven to be very useful to test different domains of the available phase space of parameters and has led us to important conclusions for the ongoing development of the code for hadronic collisions.

5.2 Analysis

We have booked histograms for all the above distributions in the same bins as the experimental data. For a given bin i we then compare the data D_i value with the Herwig++ Monte Carlo result M_i . Given the data errors δD_i (statistical plus systematic) and Monte Carlo errors δM_i (statistical only), we can calculate a χ^2 for each observable. We keep the statistical error of the Monte Carlo generally smaller than the experimental error. In distributions where the normalization is not fixed, such as momentum spectra, we allow the normalization of the Monte Carlo to be free to minimize χ^2 . The normalization is then tested separately against the average multiplicity. In all other cases we normalize histograms to unity.

As we do not want to put too much emphasis on a single observable or a particular region in phase space where the data are very precise, in computing χ^2 we set the relative experimental error in each bin to $\max(\delta D_i/D_i, 5\%)$. This takes into account the fact that the Monte Carlo is only an approximation to QCD and agreement with the data within 5% would be entirely satisfactory. The general trend for the preferred range of a single parameter was however never altered by this procedure.

After normalization the ratio

$$R_i = \frac{M_i - D_i}{D_i} \pm \left(\frac{\delta M_i}{D_i} \oplus \frac{M_i \delta D_i}{D_i^2} \right) \quad (5.2)$$

is computed for each bin in order to see precisely where the model fails. This ratio as well as the relative experimental error (yellow) and the relative contribution of each bin to the χ^2 of an observable is plotted below each histogram.

5.3 Strategy

We have taken χ^2 values for hadron multiplicities into account in the same way as we weighted the event shapes. In general the multiplicities of individual particle species are sensitive to a completely different set of parameters. The general strategy was to start from an initial set of hadronization parameters taken from HERWIG, and to aim for a good value for the total number of charged particles with reasonable values for the parton shower cutoff parameter δ and the maximum cluster mass parameter **CLMax**. Once these were fixed, the hadronization parameters that determine the multiplicities of individual particle species were determined. Following this we compared this ‘preferred’ set of parameters with the ‘initial’ set from HERWIG. The resulting parameter set is shown in table 1.

6. Results

We have chosen a wide range of observables in order to test different aspects of the model. Event shape variables and multiplicities are considered in order to test the dynamical aspects of parton shower and hadronization models, which are closely linked at their interface via the parton shower cutoff parameter δ . Ideally, the two models should merge smoothly at scales where $Q_g \sim 1$ GeV. All figures shown at the end of the paper contain three sets of plots:

- the actual distribution. The **Herwig++** result is plotted as a histogram together with the experimental data points (top);
- the ratio R_i (5.2) together with an error band, showing the relative experimental statistical and systematic errors (middle);
- the relative contribution of each data point to the total χ^2 of each plot (bottom).

6.1 Hadron multiplicities

Table 2 shows the results of the new algorithm in comparison with the old algorithm. The column labelled ‘Old Model’ is the result of using the old algorithm with the new shower variables. The column **Herwig++** is using the new algorithm with the new shower and the last column, labeled **Fortran**, is using the Fortran HERWIG program

(version 6.5). Data are combined and updated from a variety of sources, see ref. [22]. We see that, even before systematic tuning, the overall results are better than those of HERWIG, with fewer prediction that differ from the data by more than three standard deviations (starred).

We also considered the distribution of the charged particle multiplicity in comparison to OPAL data [23] and find fairly good agreement (fig. 3), although with some excess at low multiplicity.

6.2 Jet multiplicity

In fig. 4 we show the average number of jets $\langle n_{jets} \rangle$ at the Z^0 -pole, as a function of the Durham jet resolution y_{cut} , for various values of the cutoff parameter δ . At the parton level (top left) the jet multiplicity varies a lot as we go to small values of y_{cut} , saturating at the number of partons that are present in a single event. The order of magnitude of the visible saturation scales is characterized for each flavour by the different cutoff values Q_g as $y_{sat} = Q_g^2/Q^2$ (cf. (3.16)). During hadronization, low parton multiplicities lead to large mass clusters which tend to decay into low mass clusters below a given cutoff mass, which is fixed to its default value throughout the current section. Fig. 4 (top right) shows that the hadronization compensates for lower partonic multiplicities, giving a result insensitive to δ at the hadron level. In other words, we have a smooth interface between perturbative and non-perturbative dynamics between the lower end of the parton shower on one side and the cluster hadronization model on the other side. On the hadron level we describe LEP data from OPAL [24] well.

In order to test the sensitivity of our model against the variation of the c.m. energy, we calculate the jet multiplicities at PETRA and LEP II energies as well (fig. 4, bottom). The comparison to JADE [25] and OPAL [24] data shows a good agreement. In all runs we applied the same cutoffs on the energy of the partonic subsystem as did the experiments.

The additional curves in fig. 4 show predictions for the jet multiplicity [26] from the resummation of leading logarithms. Note that the parameter Λ_{QCD} in the resummed calculation is not $\Lambda_{\overline{MS}}$. We see that for the value $\Lambda_{QCD} = 500$ MeV there is good agreement with the data and the **Herwig++** result throughout the perturbative region, $y_{cut} > 10^{-4}$.

6.3 Jet rates and Y_n distributions

Another set of observables that is known to be well-described at LEP energies are the fractions of n -jet events at a given y_{cut} in the Durham scheme. In fig. 5 we compare the results from **Herwig++** with LEP data from [24] and find good agreement. On the hadron level these predictions are not very sensitive to the cutoff parameter δ . The 5-jet distribution is not shown and R_6 is the rate of ≥ 6 -jet events.

The Durham Y_n distributions in fig. 6 are histograms of those y_{cut} -values at which an $n + 1$ -jet is merged into an n -jet event in the Durham jet clustering scheme. We may say that they resolve more internal structure of the jets than the n -jet rates. Still, the agreement between model and data is quite good, although there is a tendency (which was also present in HERWIG) to exceed the data at low Y_n .

6.4 Event shapes

In order to test the dynamics of the parton shower in **Herwig++** in more detail we consider a set of commonly used event shape variables. Not only the collinear region of the parton shower is probed in greater detail but also the regions of phase space which are vetoed as matrix element corrections. We compare all results to DELPHI data [27].

In fig. 7 we show the distribution of thrust, thrust-major and thrust-minor. These variables are all obtained from a linear momentum tensor. The thrust distribution is shown with and without matrix element corrections switched on. The prediction without matrix element corrections is very much better than that of HERWIG, owing to the improved shower algorithm. It is interesting that the matrix element corrections seem to generate almost too much transverse structure, leading to event shapes that are less two-jet-like. On the other hand, there is also a slight excess of events close to the two-jet limit.

It is remarkable how well distributions like C and D parameter (fig. 8) which are sensitive to three- and four-jet-like events are described by our model even though we are limited to three jet matrix elements plus showers. Here again we have in fact a small excess at high values.

We show also in fig. 8 the distributions of sphericity and planarity, which are obtained from a quadratic momentum tensor and therefore put more emphasis on high momenta. As was the case for the thrust-related distributions, we tend to have slightly wide events. In addition we consider the jet broadening measures B_{max} and B_{min} and the hemisphere jet masses (fig. 9). In all cases the agreement between model and data is good.

6.5 Four jet angles

We show the four-jet angles in fig. 10. They are considered only for events where we have a four-jet event at $y_{\text{cut}} = 0.008$. Despite the fact that we do not have any matching to higher order matrix elements, as was proposed in [28] and implemented in [6], the agreement between model and data [29] is remarkably good. Even though we expected the implementation of hard and soft matrix element corrections in **Herwig++** to be most important for the description of these observables, we did not find very significant differences with or without the application of matrix element corrections.

6.6 Single particle distributions

In fig. 11 we show single charged particle distributions within the event, oriented along the thrust axis. The transverse momentum within the event plane $p_{\perp,\text{in}}^T$ is shown with and without matrix element corrections. In contrast to the thrust distribution we find that the matrix element corrections actually improve the distribution. Furthermore, $p_{\perp,\text{out}}^T$ and the rapidity along the thrust axis are rather well described. We do not show the analogous momentum distributions with respect to the sphericity axis which have similar features.

We consider the distribution of scaled momentum $x_p = 2|\mathbf{p}|/Q$ of charged particles in fig. 12. In addition to the full distribution we also consider the results from light (uds), c and b events.³ In all cases we compare with data from SLD [30]. The charged particle distribution is well described in all four cases, in fact somewhat better for heavy primary quarks.

6.7 Identified hadron spectra

As in the case of all charged particles we can compare identified particle spectra from events of different flavour to SLD data [30]. Data for π^\pm (not shown, being almost equivalent to all charged particles), K^\pm and (p, \bar{p}) are available. In fig. 13 we see the data for (p, \bar{p}) spectra from events of different flavour. For large values of x_p we clearly overshoot the data in light flavoured events. This is somewhat compensated by the heavy quark events which in turn seem to prefer lower values of x_p . We believe that this feature is related to the hadronization, being similar to but smaller than that seen in HERWIG.

Fig. 14 shows distributions for K^\pm and $\Lambda, \bar{\Lambda}$. Both are rather better described than the proton spectra but the distribution of $\Lambda, \bar{\Lambda}$ tends to have a similar, though smaller, ‘bump’ in comparison to data from ALEPH [31].

6.8 B fragmentation function

In fig. 15 we consider the B hadron fragmentation function in comparison to data from SLD [32]. We have also considered data from ALEPH [33] (not shown). We can describe the data quite well without any additional tuning of the hadronization model to this data. The parton shower formulation in terms of the new variables [10] and taking quark masses in the splitting functions into account clearly improves the description of heavy quark events.

6.9 Overall results

In table 3 we show a list of χ^2 values for all observables that were studied during our analysis, including those not shown in the plots. The most sensitive parameters were the cutoff value δ and the use of (hard plus soft) matrix element corrections.

³The flavour of the quark-antiquark produced in the initial hard process.

The table shows three values of δ : our preferred value of $\delta = 2.3 \text{ GeV}$ as well as the lowest and highest values that we considered.

The results should be interpreted with care. The overall trend suggests that we should prefer a large cutoff scale. However, we have just averaged over all possible observables. Taking a closer look, we may want to weight different observables in a different way.

In more detail, the general trend is the following: event shapes, jet rates and differential jet rates prefer a low cutoff. The single particle distributions along the thrust and sphericity axes prefer a small cutoff value. The y_{nm} distributions prefer either a high or a low cutoff value. The spectra of identified particles tend to prefer the high cutoff value with some exceptions for light quark events. The B fragmentation function clearly prefers the intermediate value.

In addition, as indicated in sec. 5.3, we found that the measured yields of identified particles clearly prefer the value $\delta = 2.3 \text{ GeV}$.

7. Conclusions

We have achieved a complete event generator for e^+e^- annihilation into hadrons. The main physics features, in comparison to the previous versions of HERWIG, are an improved parton shower, capable of properly describing the perturbative splitting of heavy quarks, and an improved cluster hadronization model.

We have tested our model against a wide range of data from e^+e^- colliders and are able to give a good general description of the data.

For many observables the description of the data has been improved with respect to HERWIG. The new parton shower has a number of remarkable features. The need for matrix element corrections has decreased. The main reason for this is the use of improved splitting functions, which give a far better approximation of the matrix elements in the region of collinear gluon emissions. We can describe observables involving light or heavy quark splitting with a unique set of parameters. The new hadronization model also improves the description of identified particle spectra and multiplicities.

The detailed analysis of our results leaves us with a *recommendation*: the set of parameters that is shown in table 1. This set of parameters is understood as a weighted compromise in order to give a good overall description of the data we have considered so far. We did not aim at a complete tuning of the model, but rather wanted to study its ability to describe the broad features of the data, which turned out to be very successful.

Future work on the program will extend the parton shower to initial state radiation and include a model for the soft underlying event in hadron-hadron collisions, aiming at a complete event generator for the simulation of Tevatron and LHC events.

Acknowledgments

We would like to thank Leif Lönnblad for constantly supporting ThePEG and for many useful conversations. We also thank Peter Richardson for very fruitful discussions and comments. Many thanks to Klaus Hamacher, Hendrik Hoeth and Günther Dissertori for providing us with four-jet data. S.G. and P.S. would like to thank the CERN Theory Division for hospitality while part of this work was done. S.G. would like to thank Frank Krauss and David Ward for fruitful conversations. This work was supported by the UK Particle Physics and Astronomy Research Council.

References

- [1] G. Corcella *et al.*, “HERWIG 6.5 release note,” arXiv:hep-ph/0210213;
G. Corcella *et al.*, “HERWIG 6: An event generator for hadron emission reactions with interfering gluons (including supersymmetric processes),”
JHEP **0101** (2001) 010 [arXiv:hep-ph/0011363].
- [2] T. Sjostrand, L. Lonnblad, S. Mrenna and P. Skands, “PYTHIA 6.3 physics and manual,” arXiv:hep-ph/0308153; T. Sjostrand, P. Eden, C. Friberg, L. Lonnblad, G. Miu, S. Mrenna and E. Norrbin, “High-energy-physics event generation with PYTHIA 6.1,” Comput. Phys. Commun. **135** (2001) 238 [arXiv:hep-ph/0010017].
- [3] M. Bertini, L. Lonnblad and T. Sjostrand, “Pythia version 7-0.0: A proof-of-concept version,” Comput. Phys. Commun. **134** (2001) 365 [arXiv:hep-ph/0006152].
- [4] <http://www.physik.tu-dresden.de/~krauss/hep/>.
- [5] S. Gieseke, A. Ribon, M.H. Seymour, P. Stephens and B.R. Webber, “Herwig++ 1.0, Physics and Manual,” preprint Cavendish-HEP-03/20, in preparation.
- [6] R. Kuhn, F. Krauss, B. Ivanyi and G. Soff, “APACIC++ 1.0: A Parton Cascade In C++,” Comput. Phys. Commun. **134** (2001) 223 [arXiv:hep-ph/0004270];
F. Krauss, R. Kuhn and G. Soff, “AMEGIC++ 1.0: A matrix element generator in C++,” JHEP **0202** (2002) 044 [arXiv:hep-ph/0109036].
- [7] <http://http://www.thep.lu.se/ThePEG/>.
- [8] L. Lonnblad, “CLHEP: A project for designing a C++ class library for high-energy physics,” Comput. Phys. Commun. **84** (1994) 307;
<http://wwwasd.web.cern.ch/wwwasd/lhc++/clhep/>.
- [9] R. K. Ellis, W. J. Stirling and B. R. Webber, “QCD and Collider Physics,”
Cambridge Monogr. Part. Phys. Nucl. Phys. Cosmol. **8** (1996) 1.
- [10] S. Gieseke, P. Stephens and B. Webber, “New formalism for QCD parton showers,”
arXiv:hep-ph/0310083.

- [11] B. R. Webber, “A QCD Model For Jet Fragmentation Including Soft Gluon Interference,” Nucl. Phys. B **238** (1984) 492; G. Marchesini and B. R. Webber, “Monte Carlo Simulation Of General Hard Processes With Coherent QCD Radiation,” Nucl. Phys. B **310** (1988) 461.
- [12] A. Kupco, “Cluster hadronization in HERWIG 5.9,” in Proc. *Monte Carlo generators for HERA physics*, (Hamburg 1998–1999), eds. A.T. Doyle, G. Grindhammer, G. Ingelman, H. Jung. Hamburg, DESY-PROC-1999-02, 292 [arXiv:hep-ph/9906412].
- [13] J. C. Winter, F. Krauss and G. Soff, “A modified cluster-hadronization model,” arXiv:hep-ph/0311085.
- [14] R. Kleiss, “From two to three jets in heavy boson decays: an algorithmic approach,” Phys. Lett. B **180** (1986) 400; M. H. Seymour, “A simple prescription for first order corrections to quark scattering and annihilation processes,” Nucl. Phys. B **436** (1995) 443 [arXiv:hep-ph/9410244].
- [15] S. Catani, S. Dittmaier, M. H. Seymour and Z. Trocsanyi, “The dipole formalism for next-to-leading order QCD calculations with massive partons,” Nucl. Phys. B **627** (2002) 189 [arXiv:hep-ph/0201036].
- [16] P. Richardson, “Spin correlations in Monte Carlo simulations,” JHEP **0111** (2001) 029 [arXiv:hep-ph/0110108].
- [17] M. H. Seymour, “Matrix element corrections to parton shower algorithms,” Comput. Phys. Commun. **90** (1995) 95 [arXiv:hep-ph/9410414].
- [18] D. Amati and G. Veneziano, “Preconfinement as a property of perturbative QCD,” Phys. Lett. B **83** (1979) 87.
- [19] Yu. L. Dokshitzer, contribution at *Workshop on Jet Studies at LEP and HERA*, Durham, December 1990, cited in W. J. Stirling, “Hard QCD Working Group: Theory Summary,” J. Phys. G **17** (1991) 1567; S. Catani, Y. L. Dokshitzer, M. Olsson, G. Turnock and B. R. Webber, “New clustering algorithm for multi-jet cross-sections in e^+e^- annihilation,” Phys. Lett. B **269** (1991) 432.
- [20] J. M. Butterworth, J. P. Couchman, B. E. Cox and B. M. Waugh, “KtJet: A C++ implementation of the K(T) clustering algorithm,” Comput. Phys. Commun. **153** (2003) 85 [arXiv:hep-ph/0210022].
- [21] A. Heister *et al.* [ALEPH Collaboration], “Measurements of the strong coupling constant and the QCD colour factors using four-jet observables from hadronic Z decays,” Eur. Phys. J. C **27** (2003) 1.
- [22] I. G. Knowles and G. D. Lafferty, “Hadronization in Z0 decay,” J. Phys. G **23** (1997) 731 [arXiv:hep-ph/9705217]; B. R. Webber, in *Proc. of the 19th Intl. Symp. on Photon and Lepton Interactions at High Energy LP99* ed. J.A. Jaros and M.E. Peskin, Int. J. Mod. Phys. A **15S1** (2000) 577 [eConf **C990809** (2000) 577] [arXiv:hep-ph/9912292]; R.J. Hemingway, private communication.

- [23] P. D. Acton *et al.* [OPAL Collaboration], “A Study of charged particle multiplicities in hadronic decays of the Z0,” Z. Phys. C **53** (1992) 539.
- [24] P. Pfeifenschneider *et al.* [JADE collaboration], “QCD analyses and determinations of α_s in e^+e^- annihilation at energies between 35 GeV and 189 GeV,” Eur. Phys. J. C **17** (2000) 19 [arXiv:hep-ex/0001055].
- [25] P. A. Movilla Fernandez, O. Biebel, S. Bethke, S. Kluth and P. Pfeifenschneider [JADE Collaboration], “A study of event shapes and determinations of α_s using data of e^+e^- annihilations at $\sqrt{s} = 22$ GeV to 44 GeV,” Eur. Phys. J. C **1** (1998) 461 [arXiv:hep-ex/9708034].
- [26] S. Catani, Y. L. Dokshitzer, F. Fiorani and B. R. Webber, “Average multiplicities in two and three jet e^+e^- annihilation events,” Nucl. Phys. B **383** (1992) 419; “Average number of jets in e^+e^- annihilation,” Nucl. Phys. B **377** (1992) 445.
- [27] P. Abreu *et al.* [DELPHI Collaboration], “Tuning and test of fragmentation models based on identified particles and precision event shape data,” Z. Phys. C **73** (1996) 11.
- [28] S. Catani, F. Krauss, R. Kuhn and B. R. Webber, “QCD matrix elements + parton showers,” JHEP **0111** (2001) 063 [arXiv:hep-ph/0109231].
- [29] H. Hoeth, “Messung der Vierjet–Winkelverteilungen und Bestimmung der QCD–Farbfaktoren mit Hilfe des Apac++–Generators,” Diploma Thesis, Fachbereich Physik, Bergische Universität Wuppertal, 2003 [WUD 03-11].
- [30] K. Abe *et al.* [SLD Collaboration], “Production of π^+ , π^- , K^+ , K^- , p and anti- p in light (uds), c and b jets from Z0 decays,” arXiv:hep-ex/0310017.
- [31] R. Barate *et al.* [ALEPH Collaboration], “Studies of quantum chromodynamics with the ALEPH detector,” Phys. Rept. **294** (1998) 1.
- [32] K. Abe *et al.* [SLD Collaboration], “Measurement of the b -quark fragmentation function in Z0 decays,” Phys. Rev. D **65** (2002) 092006 [Erratum-ibid. D **66** (2002) 079905] [arXiv:hep-ex/0202031].
- [33] A. Heister *et al.* [ALEPH Collaboration], “Study of the fragmentation of b quarks into B mesons at the Z peak,” Phys. Lett. B **512** (2001) 30 [arXiv:hep-ex/0106051].

Parameter	Preferred	Initial
$\alpha_s(M_Z)$	0.118	0.114
δ/GeV	2.3	—
m_g/GeV	0.750	—
Q_{\min}/GeV in $\alpha_s(Q_{\min})$	0.631	—
$\text{Cl}_{\max}/\text{GeV}$	3.2	3.35
Cl_{pow}	2.0	—
PSplt1	1	—
PSplt2	0.33	—
B1Lim	0.0	—
ClDir1	1	—
ClDir2	1	—
ClSmr1	0.40	—
ClSmr2	0.0	—
Pwt _d	1.0	—
Pwt _u	1.0	—
Pwt _s	0.85	1.0
Pwt _c	1.0	—
Pwt _b	1.0	—
Pwt _{di}	0.55	1.0
Singlet Weight	1.0	—
Decuplet Weight	0.7	1.0

Table 1: The preferred parameters for Herwig++. The first group are shower parameters, the second are all of the hadronization parameters. In the third column we show initial values of our study, taken from HERWIG, where these differ from the preferred values.

Particle	Experiment	Measured	Old Model	Herwig++	Fortran
All Charged	M,A,D,L,O	20.924 ± 0.117	20.22*	20.814	20.532*
γ	A,O	21.27 ± 0.6	23.03	22.67	20.74
π^0	A,D,L,O	9.59 ± 0.33	10.27	10.08	9.88
$\rho(770)^0$	A,D	1.295 ± 0.125	1.235	1.316	1.07
π^\pm	A,O	17.04 ± 0.25	16.30	16.95	16.74
$\rho(770)^\pm$	O	2.4 ± 0.43	1.99	2.14	2.06
η	A,L,O	0.956 ± 0.049	0.886	0.893	0.669*
$\omega(782)$	A,L,O	1.083 ± 0.088	0.859	0.916	1.044
$\eta'(958)$	A,L,O	0.152 ± 0.03	0.13	0.136	0.106
K^0	S,A,D,L,O	2.027 ± 0.025	2.121*	2.062	2.026
$K^*(892)^0$	A,D,O	0.761 ± 0.032	0.667	0.681	0.583*
$K^*(1430)^0$	D,O	0.106 ± 0.06	0.065	0.079	0.072
K^\pm	A,D,O	2.319 ± 0.079	2.335	2.286	2.250
$K^*(892)^\pm$	A,D,O	0.731 ± 0.058	0.637	0.657	0.578
$\phi(1020)$	A,D,O	0.097 ± 0.007	0.107	0.114	0.134*
p	A,D,O	0.991 ± 0.054	0.981	0.947	1.027
Δ^{++}	D,O	0.088 ± 0.034	0.185	0.092	0.209*
Σ^-	O	0.083 ± 0.011	0.063	0.071	0.071
Λ	A,D,L,O	0.373 ± 0.008	0.325*	0.384	0.347*
Σ^0	A,D,O	0.074 ± 0.009	0.078	0.091	0.063
Σ^+	O	0.099 ± 0.015	0.067	0.077	0.088
$\Sigma(1385)^\pm$	A,D,O	0.0471 ± 0.0046	0.057	0.0312*	0.061*
Ξ^-	A,D,O	0.0262 ± 0.001	0.024	0.0286	0.029
$\Xi(1530)^0$	A,D,O	0.0058 ± 0.001	0.026*	0.0288*	0.009*
Ω^-	A,D,O	0.00125 ± 0.00024	0.001	0.00144	0.0009
$f_2(1270)$	D,L,O	0.168 ± 0.021	0.113	0.150	0.173
$f_2'(1525)$	D	0.02 ± 0.008	0.003	0.012	0.012
D^\pm	A,D,O	0.184 ± 0.018	0.322*	0.319*	0.283*
$D^*(2010)^\pm$	A,D,O	0.182 ± 0.009	0.168	0.180	0.151*
D^0	A,D,O	0.473 ± 0.026	0.625*	0.570*	0.501
D_s^\pm	A,O	0.129 ± 0.013	0.218*	0.195*	0.127
$D_s^{*\pm}$	O	0.096 ± 0.046	0.082	0.066	0.043
J/Ψ	A,D,L,O	0.00544 ± 0.00029	0.006	0.00361*	0.002*
Λ_c^+	D,O	0.077 ± 0.016	0.006*	0.023*	0.001*
$\Psi'(3685)$	D,L,O	0.00229 ± 0.00041	0.001*	0.00178	0.0008*

Table 2: Multiplicities per event at 91.2 GeV. We show results from Herwig++ with the implementation of the old cluster hadronization model (Old Model) and the new model (Herwig++), and from HERWIG 6.5 shower and hadronization (Fortran). Parameter values used are given in table 1. Experiments are Aleph(A), Delphi(D), L3(L), Opal(O), Mk2(M) and SLD(S). The * indicates a prediction that differs from the measured value by more than three standard deviations.

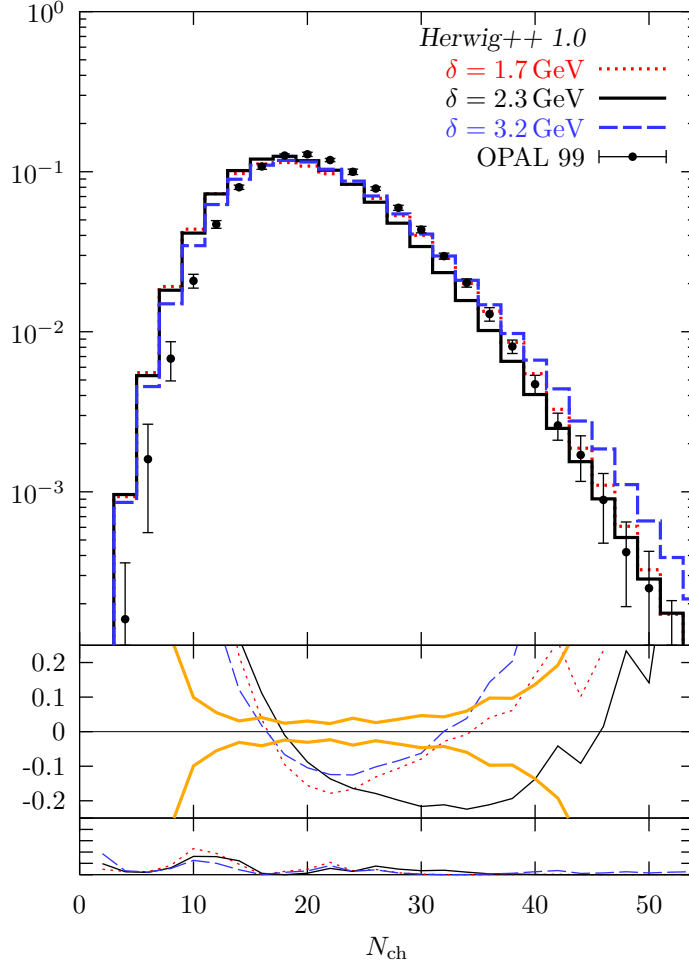


Figure 3: The distribution of the charged particle multiplicity. The three panels here and in figs. 5–15 are explained in sec. 6.

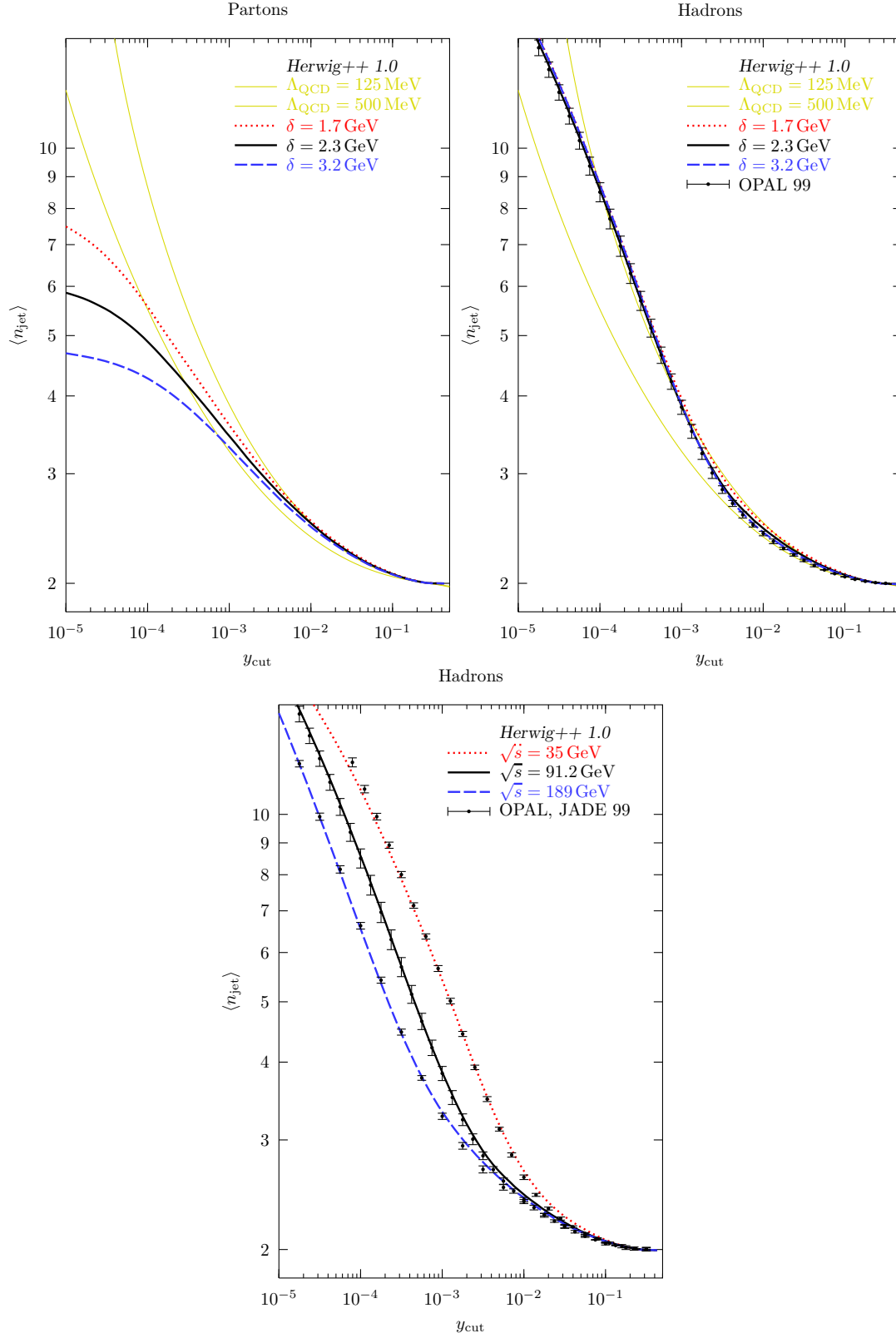


Figure 4: Jet multiplicities for different values of the cutoff parameter δ and different c.m. energies.

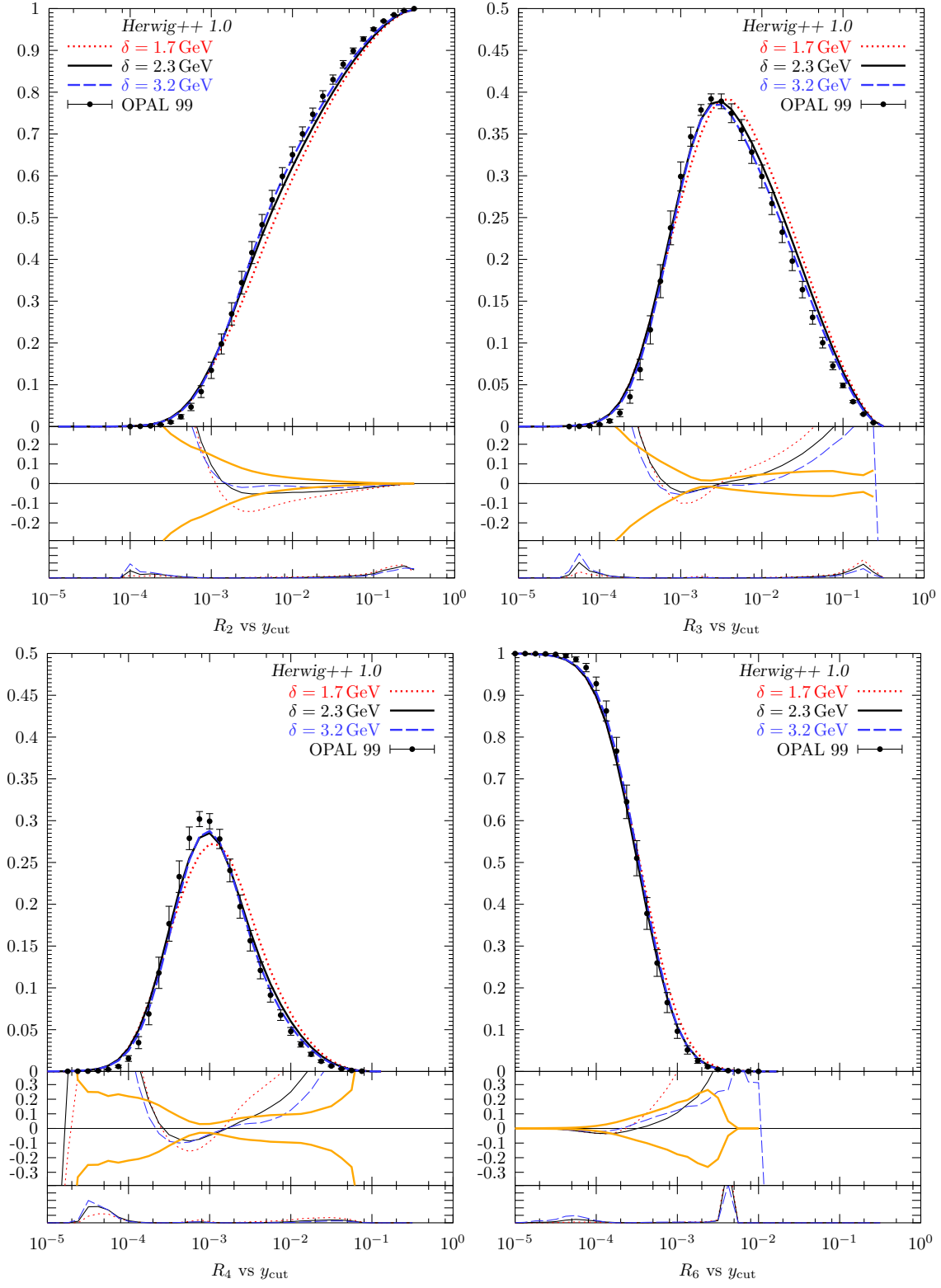


Figure 5: Jet rates in the Durham algorithm for different values of the cutoff δ .

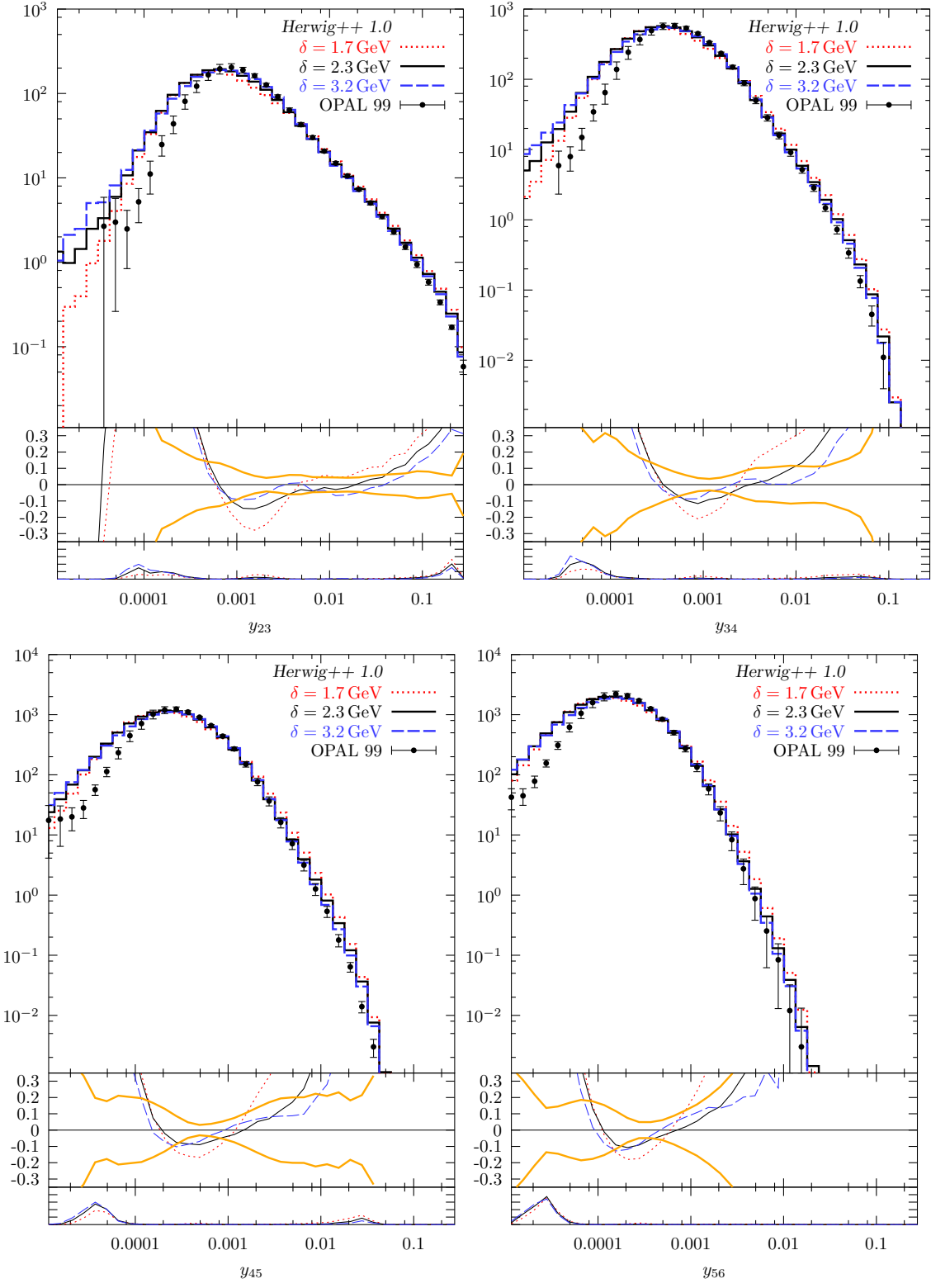


Figure 6: Durham Y_n distributions for different values of the cutoff δ .

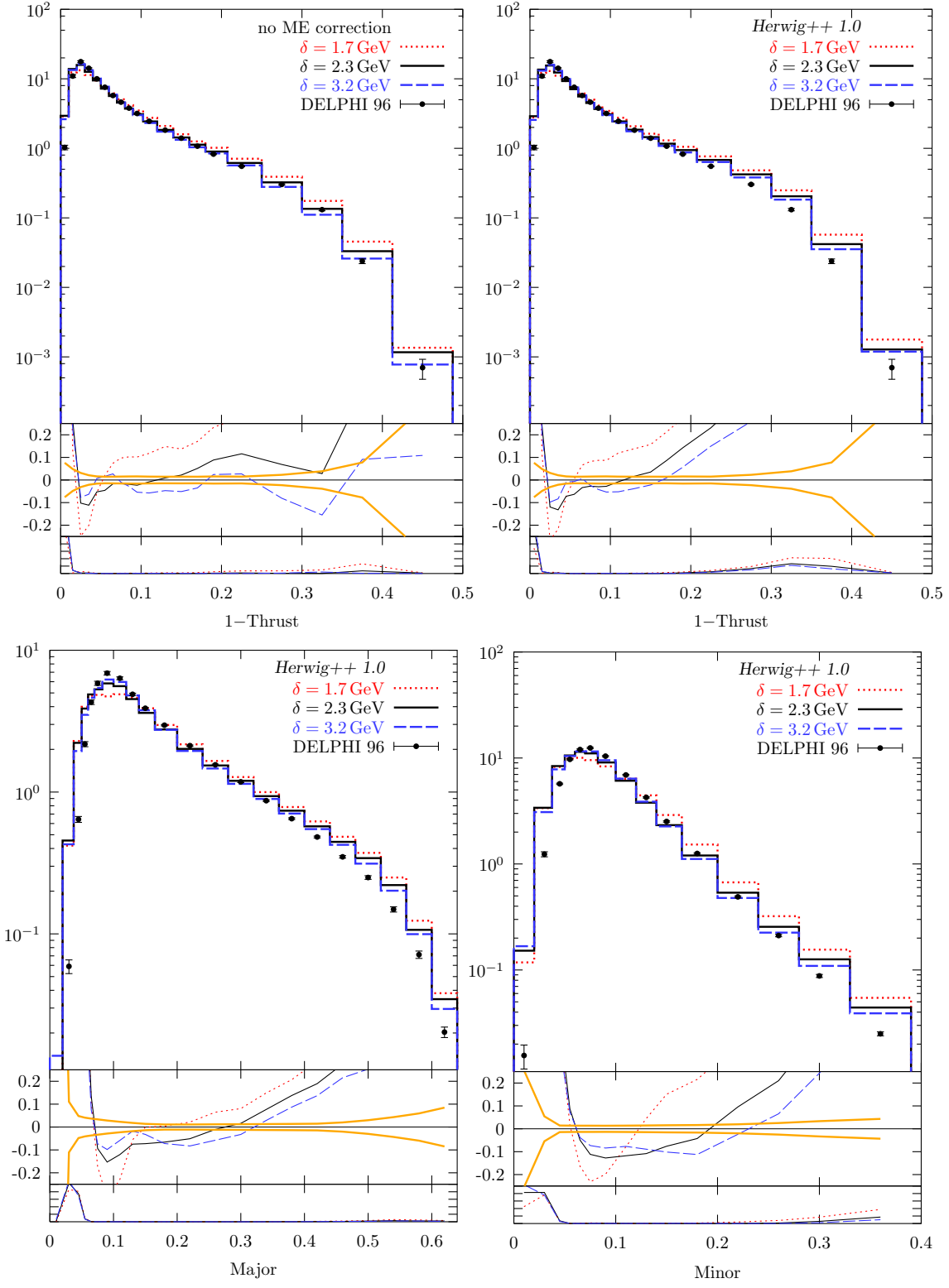


Figure 7: Thrust without (top left) and with (top right) matrix element corrections switched on, thrust major and thrust minor (bottom).

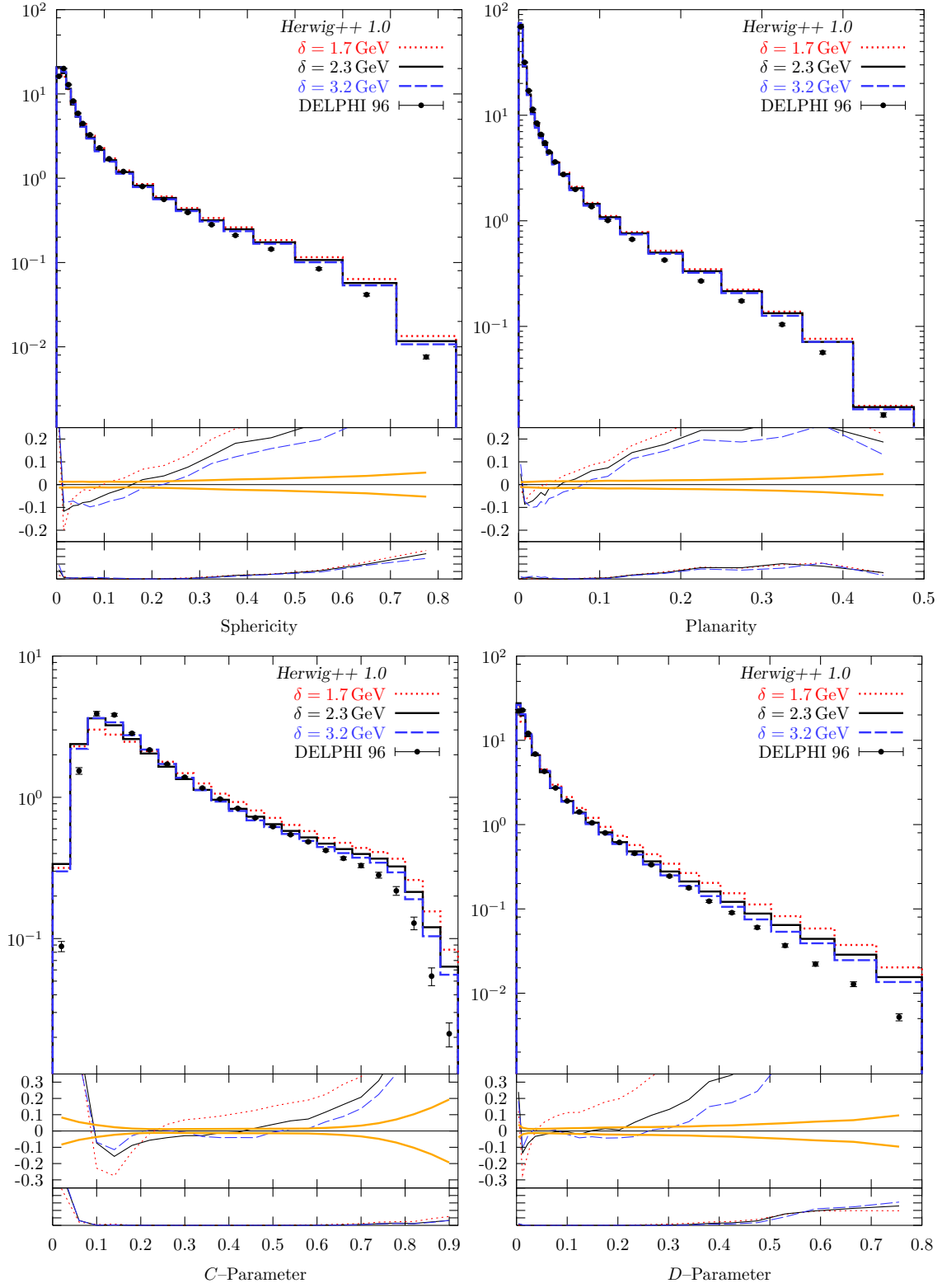


Figure 8: Sphericity, planarity, C parameter and D parameter distributions.

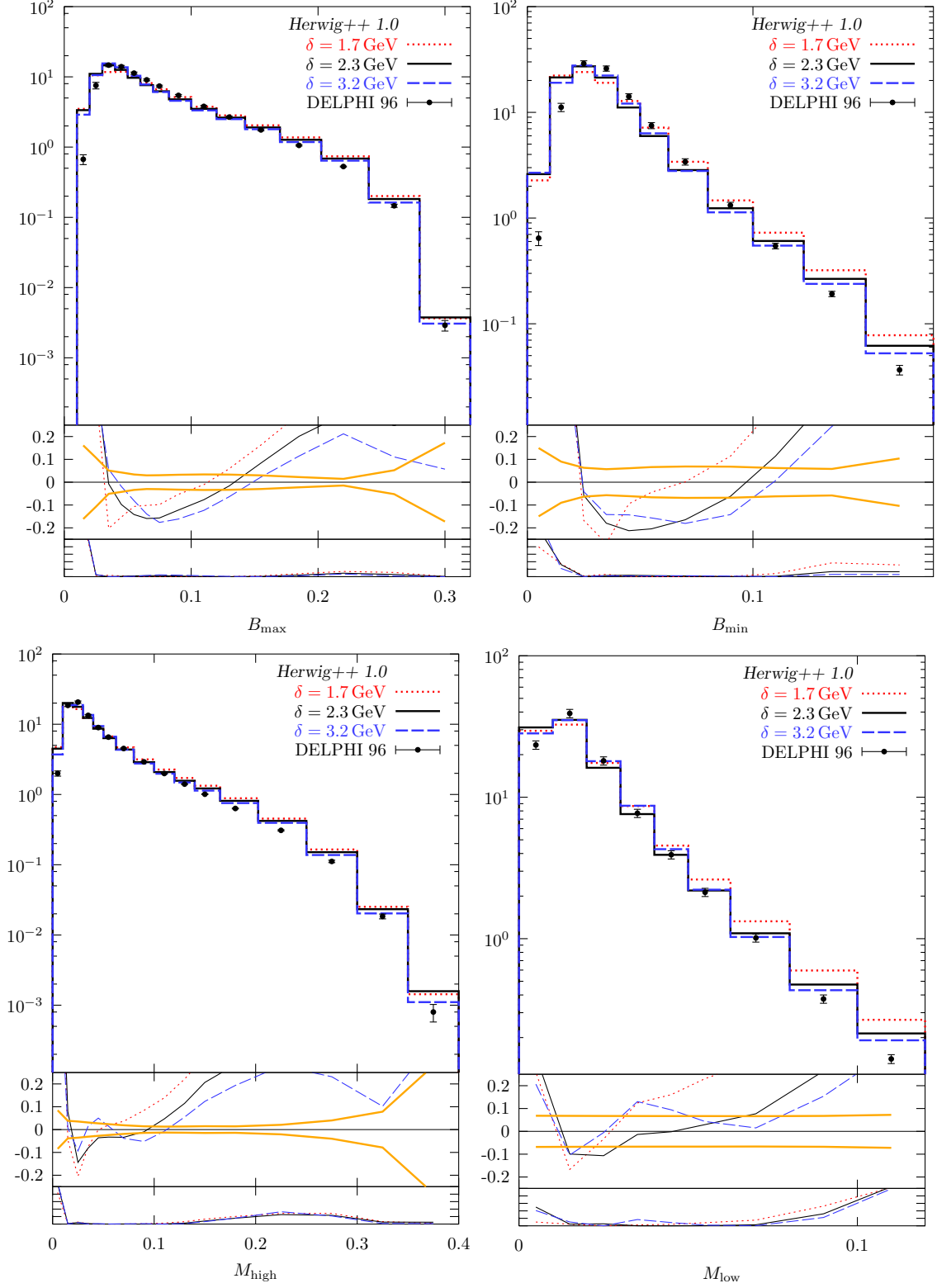


Figure 9: The wide and narrow jet broadening measures B_{\max} and B_{\min} and the high and low hemisphere masses.

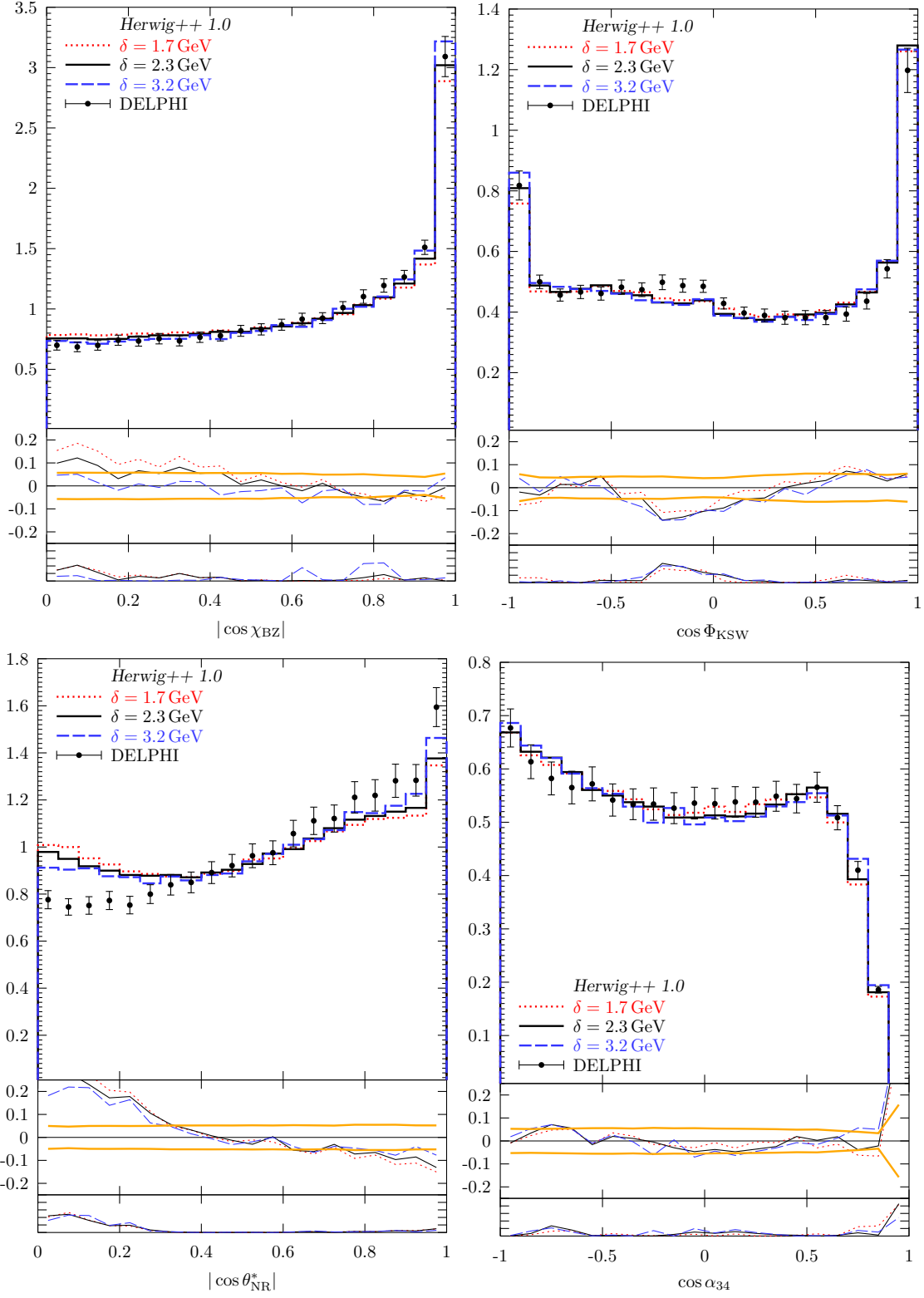


Figure 10: Four jet angle distributions. The points are from preliminary DELPHI data.

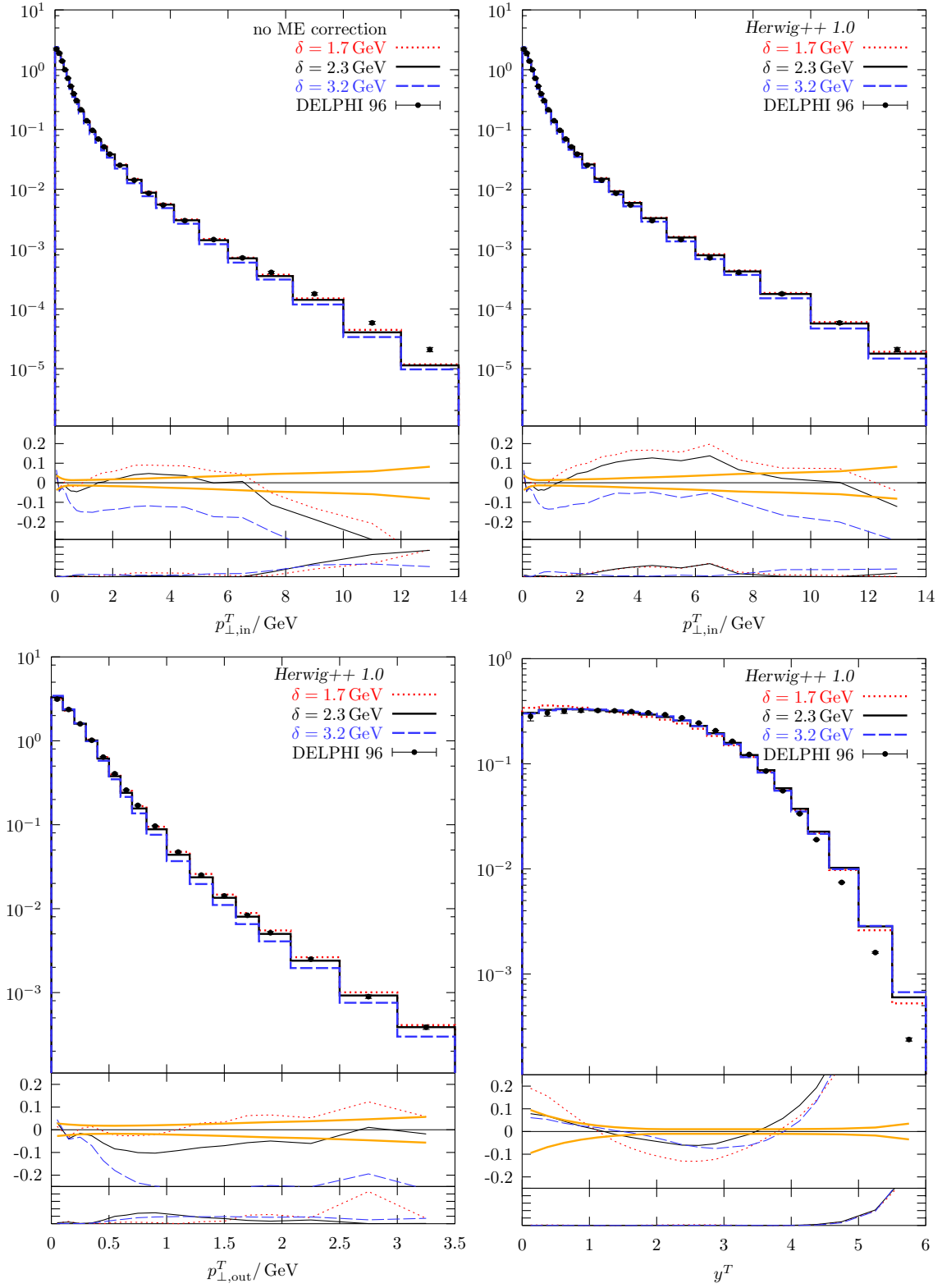


Figure 11: Momentum distributions of charged particles with respect to the thrust axis, $p_{\perp,in}^T$ (with and without matrix element corrections), $p_{\perp,out}^T$ and y^T .

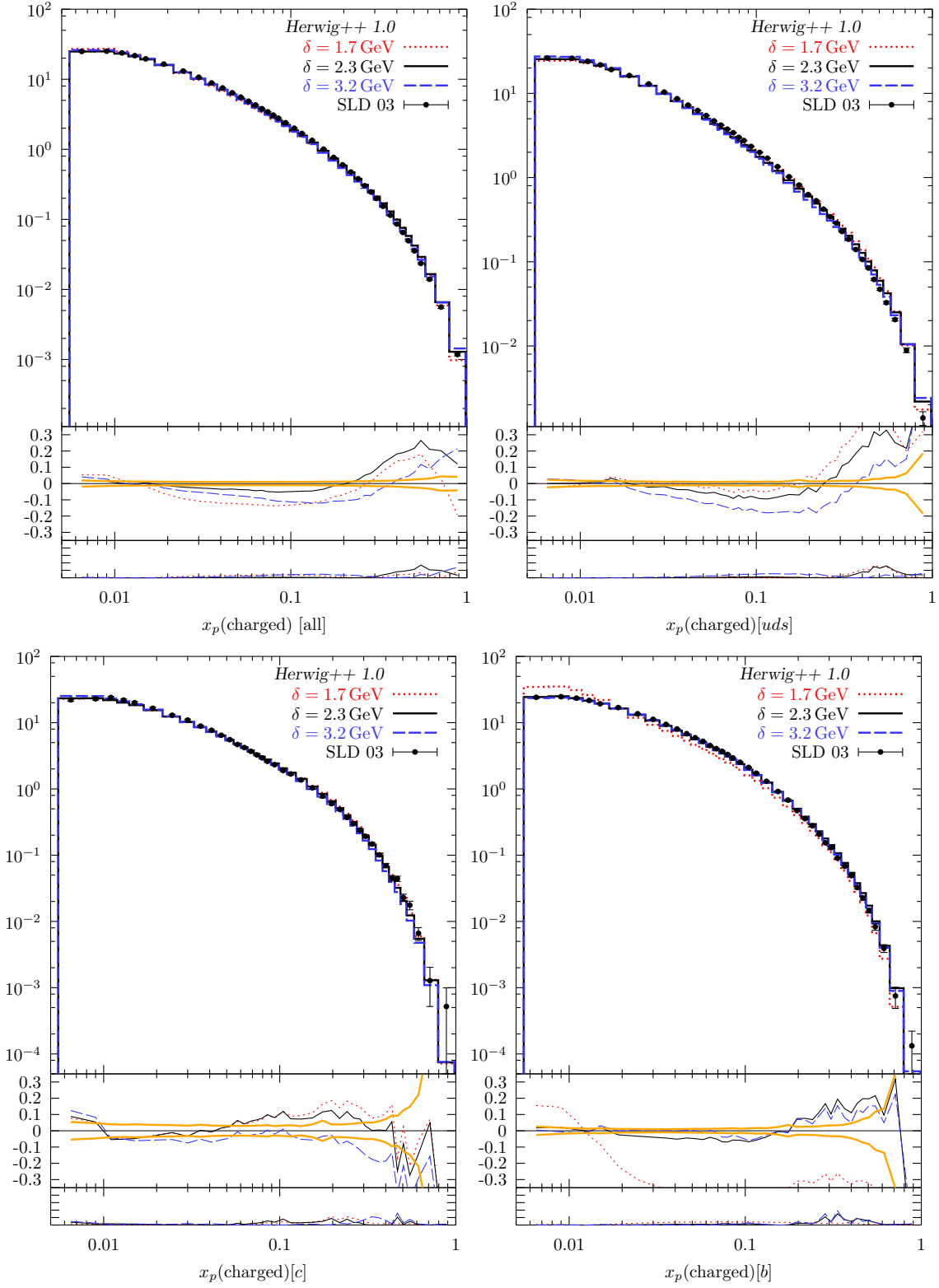


Figure 12: The scaled momentum distribution x_p of charged particles for all events as well as for uds , c and b events separately.

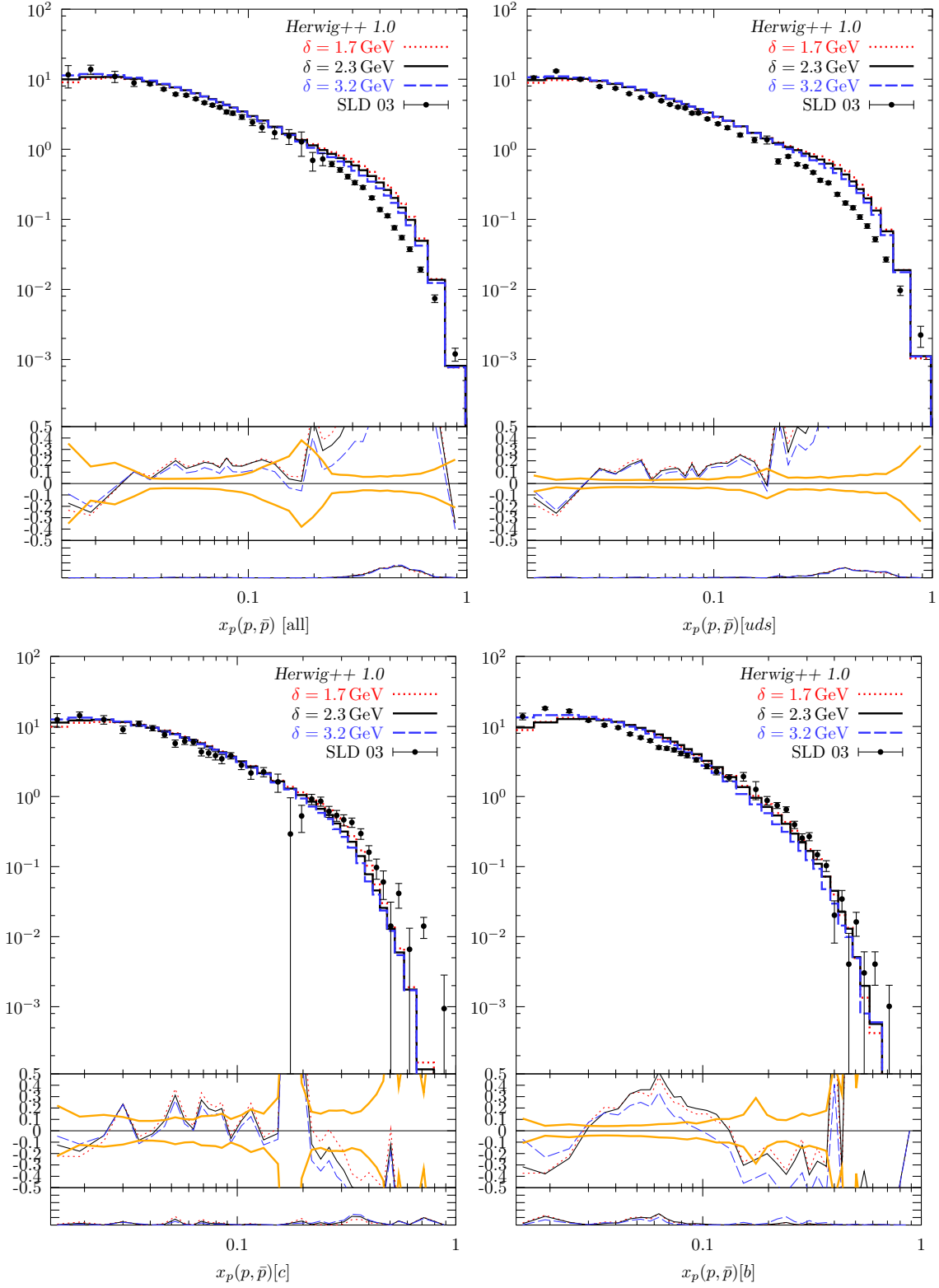


Figure 13: The scaled momentum distribution x_p of protons, shown separately for all events as well as for uds , c and b events.

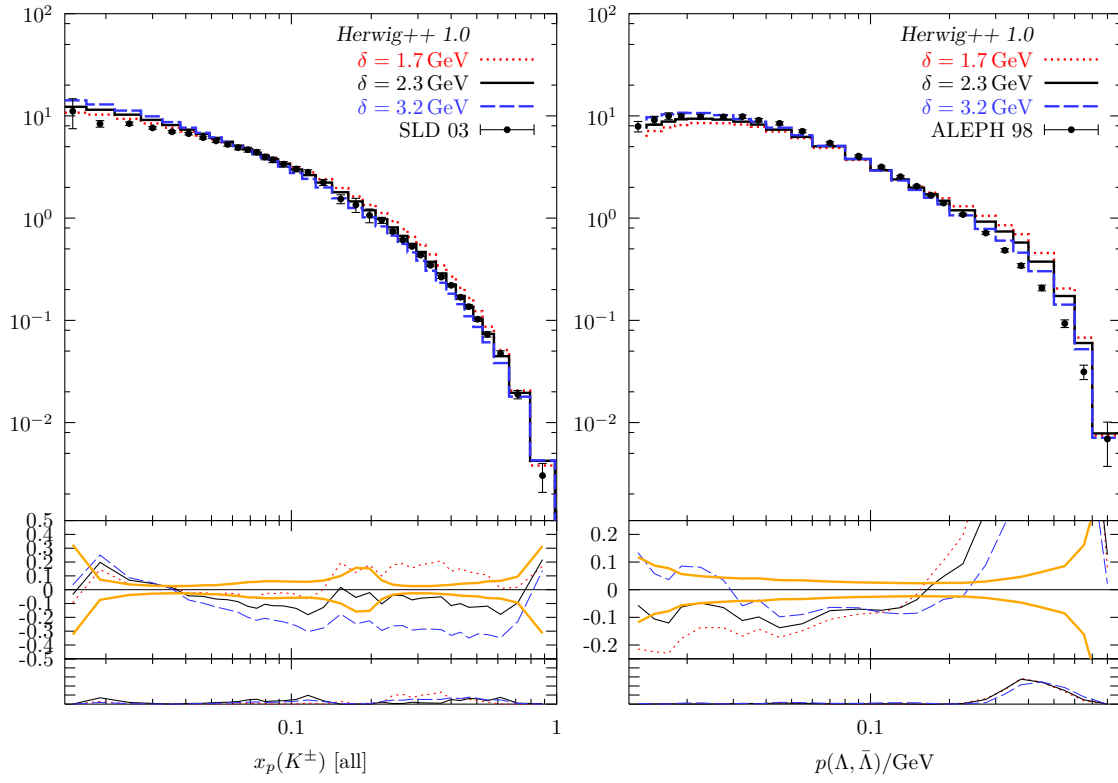


Figure 14: Distribution of scaled kaon momentum and $\Lambda, \bar{\Lambda}$ momentum.

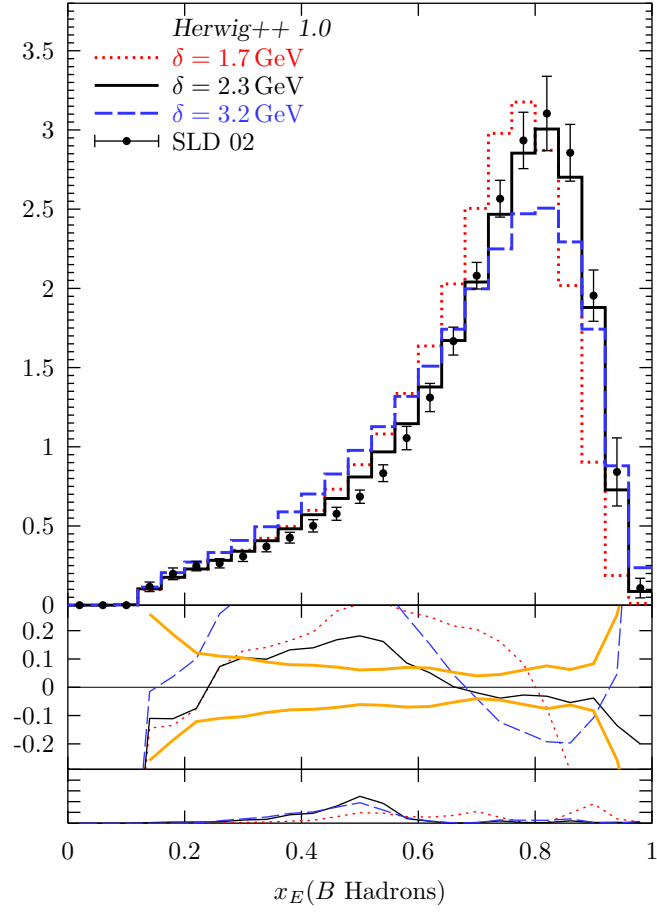


Figure 15: The B -hadron fragmentation function for different values of the cutoff δ .

Observable	Ref.	ME corrections off			ME corrections on		
		$\delta = 1.7 \text{ GeV}$	$\delta = 2.3 \text{ GeV}$	$\delta = 3.2 \text{ GeV}$	$\delta = 1.7 \text{ GeV}$	$\delta = 2.3 \text{ GeV}$	$\delta = 3.2 \text{ GeV}$
$1 - T$	[27]	44.65	33.15	22.29	72.80	45.57	26.34
M	[27]	246.25	273.42	198.37	275.80	274.43	186.34
m	[27]	150.74	157.91	137.43	174.29	163.02	129.10
O	[27]	7.41	5.58	5.14	22.24	19.33	13.34
S	[27]	4.42	3.50	4.07	24.70	14.10	8.50
P	[27]	4.48	5.63	6.54	10.69	7.40	5.62
A	[27]	19.52	10.80	7.17	44.83	20.26	11.33
C	[27]	66.86	59.26	39.56	81.41	67.44	43.08
D	[27]	84.23	29.30	12.36	161.90	60.42	26.92
M_{high}	[27]	25.78	18.88	12.38	38.43	25.69	11.52
M_{low}	[27]	15.25	5.37	2.50	31.53	10.42	5.00
M_{diff}	[27]	7.28	5.27	7.25	18.32	12.17	4.61
B_{max}	[27]	54.48	50.29	38.91	59.61	49.92	33.23
B_{min}	[27]	53.25	55.72	53.18	64.52	58.08	50.64
B_{sum}	[27]	102.29	97.35	74.60	121.86	103.10	70.98
B_{diff}	[27]	8.28	5.42	4.70	18.39	13.64	6.09
$p_{\perp, \text{in}}^T$	[27]	2.48	3.11	11.52	3.39	1.70	4.26
$p_{\perp, \text{out}}^T$	[27]	0.25	3.28	21.65	0.80	1.70	16.06
y^T	[27]	34.52	60.55	66.05	34.94	53.81	59.07
$p_{\perp, \text{in}}^S$	[27]	2.53	3.19	11.76	2.32	1.39	4.30
$p_{\perp, \text{out}}^S$	[27]	0.37	3.77	22.64	0.90	2.01	16.78
y^S	[27]	9.04	17.49	24.85	7.78	14.72	21.94
D_2^D	[27]	9.37	3.54	3.76	25.56	11.27	5.25
D_3^D	[27]	25.85	6.33	2.14	47.11	15.31	5.42
D_4^D	[27]	43.90	10.47	2.69	78.82	23.26	7.11
y_{23}	[24]	8.75	6.11	5.36	12.35	8.65	6.40
y_{34}	[24]	10.20	9.65	9.07	11.46	10.02	8.81
y_{45}	[24]	15.53	14.40	11.78	17.74	15.57	11.75
y_{56}	[24]	16.02	17.77	15.13	15.50	17.51	14.32
$\langle N_{\text{jets}} \rangle$	[24]	12.84	3.30	0.62	28.29	12.80	5.95
R_2	[24]	9.75	6.56	6.18	19.84	13.45	9.59
R_3	[24]	10.46	8.51	9.36	23.49	15.86	11.95
R_4	[24]	13.47	10.95	10.36	15.26	12.42	10.22
R_5	[24]	25.53	24.98	23.43	28.09	26.35	22.30
R_6	[24]	10.37	1.74	0.67	18.38	4.33	1.47
$\cos(\chi_{\text{BZ}})$	[29]	2.90	1.10	0.48	2.48	1.05	0.53
$\cos(\Phi_{\text{KSW}})$	[29]	2.30	2.06	2.56	1.22	1.50	1.64
$\cos(\theta_{\text{NR}}^*)$	[29]	7.68	5.06	2.72	8.66	6.22	3.57
$\cos(\alpha_{34})$	[29]	1.41	1.57	1.71	0.60	0.64	0.76
N_{ch}	[23]	21.86	25.71	12.90	19.81	22.84	12.97
$x_p(\text{ch})[\text{all}]$	[30]	5.32	5.65	3.49	4.75	4.10	3.02
$x_p(\text{ch})[uds]$	[30]	15.72	8.50	6.13	12.63	6.69	5.86
$x_p(\text{ch})[c]$	[30]	3.95	2.29	2.17	2.96	1.76	2.73
$x_p(\text{ch})[b]$	[30]	35.05	3.23	1.79	35.79	2.49	1.22
$x_p(\pi^\pm)[\text{all}]$	[30]	8.29	9.27	6.18	7.21	7.50	5.51
$x_p(\pi^\pm)[uds]$	[30]	28.30	15.92	10.47	24.05	13.29	9.46
$x_p(\pi^\pm)[c]$	[30]	4.65	2.99	1.38	3.67	2.28	1.62
$x_p(\pi^\pm)[b]$	[30]	49.13	3.14	1.56	49.44	3.57	2.02
$x_p(K^\pm)[\text{all}]$	[30]	4.99	2.02	15.38	3.67	2.88	17.37
$x_p(K^\pm)[uds]$	[30]	6.46	17.05	36.45	6.83	19.36	38.79
$x_p(K^\pm)[c]$	[30]	21.01	2.20	3.35	18.16	1.75	4.14
$x_p(K^\pm)[b]$	[30]	8.56	7.14	4.34	7.63	5.84	4.97
$x_p(p, \bar{p})[\text{all}]$	[30]	143.34	98.19	42.90	140.48	87.08	36.23
$x_p(p, \bar{p})[uds]$	[30]	145.35	102.51	52.78	139.85	91.07	45.10
$x_p(p, \bar{p})[c]$	[30]	2.26	2.41	2.86	2.34	2.48	2.85
$x_p(p, \bar{p})[b]$	[30]	11.26	13.71	8.12	11.47	13.54	8.31
$p(\Lambda, \Lambda)$	[31]	58.02	28.52	9.47	55.27	25.50	7.86
$x_E(B)$	[32]	8.93	0.92	8.16	9.44	1.39	9.92
$x_E(B)$	[33]	15.40	1.75	7.35	15.76	2.01	8.21
$\langle \chi^2 \rangle / \text{bin}$		32.75	25.84	20.93	40.69	28.41	20.56

Table 3: χ^2/bin for all observables we studied and a relevant subset of parameters.